

Phase-modulated superconductivity via altermagnetism

Shuntaro Sumita,^{1,2,3,*} Makoto Naka,⁴ and Hitoshi Seo³

¹*Department of Basic Science, The University of Tokyo, Meguro, Tokyo 153-8902, Japan*

²*Komaba Institute for Science, The University of Tokyo, Meguro, Tokyo 153-8902, Japan*

³*RIKEN Center for Emergent Matter Science, Wako, Saitama 351-0198, Japan*

⁴*School of Science and Engineering, Tokyo Denki University, Ishizaka, Saitama 350-0394, Japan*
(Dated: June 30, 2025)

Stimulated by recent interest in altermagnets, a novel class of antiferromagnets with macroscopic time-reversal symmetry breaking, we investigate the coexistence of altermagnetism and superconductivity. By developing a Ginzburg–Landau theory based on microscopic models, we show that a *phase*-modulated Fulde–Ferrell superconducting state is stabilized via altermagnetic spin splitting, in contrast to the typical *amplitude*-modulated states that occur under a uniform Zeeman field. We apply our framework to different models: a two-sublattice model with altermagnetic order, a continuum model with an anisotropic Zeeman field mimicking altermagnetic spin splitting, and a conventional square-lattice model with two kinds of anisotropic Zeeman fields. Our results indicate that the multi-sublattice structure is crucial for realizing this exotic superconductivity, and highlight spin-split altermagnets as a promising platform for exploring phase-modulated superconductivity without external magnetic fields.

I. INTRODUCTION

Theoretical findings of characteristic properties in collinear Néel-type antiferromagnets such as spin-split dispersion relation in electronic [1–5] and magnon [4] bands, leading to spin current generation [3, 4], and the anomalous Hall effect [6–8] led to the concept of ‘altermagnetism’ [9, 10], which is now attracting significant interest. Altermagnets exhibit macroscopic time-reversal symmetry breaking below the Néel temperature because the distinct sublattices hosting up and down spins are connected not by inversion or any translation operation but by other space group operations (such as rotation, screw, or glide). A wide variety of materials is considered as their candidates: rutiles [1, 3, 7], organic antiferromagnets κ -(ET)₂X [4, 8, 11], perovskites [2, 6, 12, 13], and MnTe [14–18]. Systems showing magnetic octupole order [19–22] are also relevant to the study of altermagnets.

One of the intriguing subjects is the coexistence of altermagnetism and superconductivity. Indeed, recent theoretical studies have proposed that an altermagnetic order can induce Fulde–Ferrell–Larkin–Ovchinnikov (FFLO) superconductivity [23, 24] or pair-density-wave (PDW) superconductivity, where the Cooper pairs possess finite center-of-mass (COM) momentum [25–35], stabilized by the altermagnetic spin splitting. Such an FFLO state in the presence of anisotropic spin splitting was proposed in the context of a spin-nematic order about a decade ago [36, 37]. A compelling point about these exotic states is that they can be realized without an external magnetic field and therefore are free from vortices, in clear contrast with the original proposal of FFLO superconductivity under external magnetic field. Here we note that the altermagnetic spin ordering, by definition as mentioned above, requires at least two sublattice degrees of freedom. Without such an ingredient, however, naively an anisotropic spin splitting can be introduced by a momentum-dependent Zeeman field, which is

somewhat artificial and sometimes confusedly used in recent literature.

An issue in the FFLO state in altermagnets is its spacial structure, which is still controversial. In general, there are various possibilities for spatially modulated superconductivity: a phase-modulated FF state [with spatially varied order parameter $\eta(\mathbf{R}) \sim e^{2i\mathbf{Q}\cdot\mathbf{R}}$], an amplitude-modulated LO state [$\eta(\mathbf{R}) \sim \cos(2\mathbf{Q}\cdot\mathbf{R})$], a bidirectional PDW state [$\eta(\mathbf{R}) \sim \cos(2\mathbf{Q}\cdot\mathbf{R}) + \cos(2\mathbf{Q}'\cdot\mathbf{R})$], etc. On the basis of the Ginzburg–Landau (GL) theory, Ref. [36] showed that the LO or bidirectional PDW state is stabilized under an anisotropic spin splitting, while Ref. [30] proposed the FF state in altermagnets. In both works, the anisotropic spin splitting is introduced by a momentum-dependent Zeeman field in the model, and the sublattice degree of freedom is not taken into account.

To address this issue, in this paper we microscopically develop the GL theory based on a *multi-sublattice* tight-binding model. As mentioned above, most of the previous studies have overlooked such a sublattice degree of freedom but instead introduced a momentum-dependent Zeeman field to describe the anisotropic spin splitting in altermagnets [26, 27, 29–35]. Here we reveal that the phase-modulated FF superconductivity, rather than amplitude-modulated states, is stabilized in the presence of altermagnetic order. This is a distinctive characteristic of altermagnets, because typically the amplitude-modulated state is more stable in most superconductors under a uniform Zeeman field [38–41]. Furthermore, we demonstrate that the multi-sublattice degree of freedom is actually essential for realizing the FF state, by comparing our multi-sublattice model with other models introducing the anisotropic Zeeman field as in the literature.

The rest of this paper is organized as follows. In Sec. II, we introduce three kinds of two-dimensional (2D) models studied here. The main target is a tetragonal model with two sublattices that is one of the minimal models for altermagnets (Sec. II A). Because of asymmetric hoppings in the two sublattices with different directions, the energy band has asymmetric spin splitting when an antiferromagnetic molecular field is switched

* s-sumita@g.ecc.u-tokyo.ac.jp

on. To uncover the effect of the multi-sublattice property, we then introduce a continuum model (Sec. II B) and a conventional square lattice model (Sec. II C). We incorporate the momentum-dependent Zeeman field by hand into both models, which lack a sublattice degree of freedom. Particularly in the conventional square lattice model, we compare the cases with $1\mathbf{k}$ - and $2\mathbf{k}$ - d -wave Zeeman fields, the latter of which more properly corresponds to the structure of anisotropic spin splitting in the two-sublattice tetragonal model. Next, on the basis of the mean-field (MF) approximation to introduce superconductivity, we microscopically derive the GL theory and compute the coefficients in the GL free energy for each model (Sec. III). The models, their spin split structures, and the resulting superconducting states are summarized in Table I. Our analyses show that, as either the molecular field or the Zeeman field is increased, the phase-modulated FF state becomes stable in the two-sublattice tetragonal model [Table I(a)] and the conventional square lattice model in a $2\mathbf{k}$ - d -wave Zeeman field [(c2)], whereas the amplitude-modulated state is stabilized in the other cases [(b) and (c1)]. These results highlight the crucial role of the multi-sublattice degree of freedom. A summary and discussion are given in Sec. IV.

II. MODELS AND ELECTRONIC STRUCTURES

In this section, we introduce the three 2D models discussed in this paper, based on which the stability of superconducting state will be investigated in the next section. For all the models, the noninteracting Hamiltonian is given by the form,

$$H_0 = \sum_{\mathbf{k}} \mathbf{C}_k^\dagger \hat{H}_0(\mathbf{k}) \mathbf{C}_k, \quad (1)$$

where the momentum-dependent Hamiltonian matrix is composed of two terms,

$$\hat{H}_0(\mathbf{k}) = \hat{H}_{\text{kin}}(\mathbf{k}) + \hat{H}_{\text{mag}}(\mathbf{k}). \quad (2)$$

The first term is the kinetic energy, and the second term represents the molecular field of the altermagnetic order or the Zeeman field. In the following subsections, we describe the two-sublattice tetragonal model (Sec. II A), the continuum model (Sec. II B), and the conventional square lattice model (Sec. II C).

A. Two-sublattice tetragonal model

1. Tight-binding Hamiltonian

First we introduce the two-sublattice tetragonal model for altermagnets, as shown in Table I(a) (cf. Refs. [42, 43]). This is a simplified model of κ -type organic compounds, an early identified system with altermagnetic spin splitting [4, 8, 11]. Since this model contains two sublattices in the unit cell, the operator in Eq. (1) is a four-component vector for each \mathbf{k} written as

$$\mathbf{C}_k = [c_{k,a\uparrow}, c_{k,a\downarrow}, c_{k,b\uparrow}, c_{k,b\downarrow}]^T, \quad (3)$$

where $c_{k,l,s}$ is the annihilation operator of electrons carrying momentum \mathbf{k} and spin s on the sublattice l ($= a, b$). The kinetic energy [the first term in Eq. (2)] is composed of the nearest-neighbor intersublattice hopping (t_1) and third-nearest-neighbor intrasublattice hopping (t_2) on a square lattice [see the second column in Table I(a)]:

$$\begin{aligned} \hat{H}_{\text{kin}}(\mathbf{k}) = & -4t_1 \cos \frac{k_x}{2} \cos \frac{k_y}{2} \hat{\tau}_1 \otimes \hat{\sigma}_0 \\ & - 2t_2 (\cos k_x \cos k_y \hat{\tau}_0 - \sin k_x \sin k_y \hat{\tau}_z) \otimes \hat{\sigma}_0, \end{aligned} \quad (4)$$

where the lattice constants are set to unity. Here $\hat{\tau}_i$ and $\hat{\sigma}_j$ are the Pauli matrices for the sublattice and spin spaces, respectively. We use the hopping parameters $(t_1, t_2) = (1, 0.2)$ throughout this paper. On the other hand, the molecular field of the altermagnetic order [the second term in Eq. (2)] breaking time-reversal symmetry is given by

$$\hat{H}_{\text{mag}} = -h \hat{\tau}_z \otimes \hat{\sigma}_z, \quad (5)$$

which does not depend on the momentum \mathbf{k} , but does on the two sublattices due to $\hat{\tau}_z$. Since the model does not contain spin-orbit coupling (SOC), we choose, without loss of generality, the molecular field along the z axis.

Note that the third-nearest-neighbor hopping t_2 in Eq. (4) has an anisotropic structure between the two sublattices. Reflecting the different orientations of the sublattices as in the κ -type organic compounds where the role of anisotropic hoppings was elucidated [4, 8, 11], the hopping amplitude is present only along the $[11]$ ($[1\bar{1}]$) direction for the a (b) sublattice; see the second column in Table I(a). This anisotropy causes the spin splitting in the energy band structure, when the molecular field [Eq. (5)] is nonzero.

The Hamiltonian does not satisfy the periodicity with respect to the translation $\mathbf{k} \rightarrow \mathbf{k} + \mathbf{K}$ with \mathbf{K} being a reciprocal lattice vector. We thus perform a unitary transformation by the following unitary matrix

$$\hat{U}_{\text{site}}(\mathbf{k}) = \begin{bmatrix} e^{ik_y/2} & 0 \\ 0 & e^{ik_x/2} \end{bmatrix}_\tau \otimes \hat{\sigma}_0, \quad (6)$$

to restore the periodicity of the Brillouin zone (BZ).

2. Symmetry and energy band structure

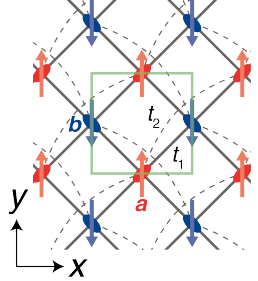
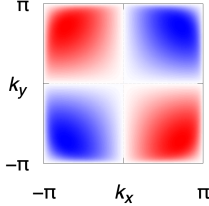
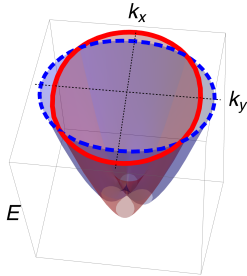
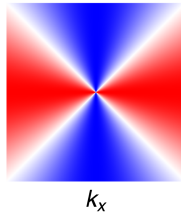
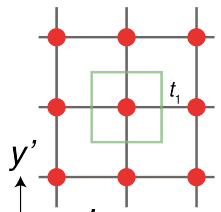
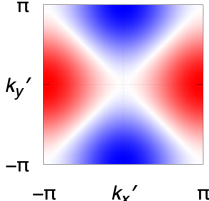
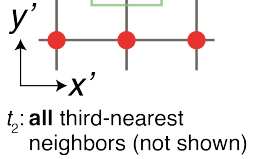
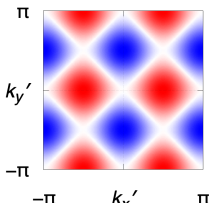
When the altermagnetic term [Eq. (5)] is absent, the model belongs to a 2D magnetic point group $4mm1'$ that is generated by fourfold rotation (C_{4z}), mirror (glide) with respect to the x axis (M_x), and time-reversal (T) symmetries [44]:

$$\hat{U}_{C_{4z}} \hat{H}_0(\mathbf{k}) \hat{U}_{C_{4z}}^\dagger = \hat{H}_0(-k_y, k_x), \quad (7a)$$

$$\hat{U}_{M_x} \hat{H}_0(\mathbf{k}) \hat{U}_{M_x}^\dagger = \hat{H}_0(-k_x, k_y), \quad (7b)$$

$$\hat{U}_T \hat{H}_0(\mathbf{k}) \hat{U}_T^\dagger = \hat{H}_0(-\mathbf{k}). \quad (7c)$$

TABLE I. Characteristics of (a) two-sublattice tetragonal, (b) continuum, and (c) conventional square lattice models considered in this paper. In the second column, we show illustrations of the square lattices for (a) and (c), where the unit cells are represented by green squares, and the energy dispersion for (b). In the third column, we refer to molecular (Zeeman) fields for anisotropic spin splitting, which depend on the momentum for (b) and (c) but not for (a). In particular, we treat (c1) $1k$ - d -wave and (c2) $2k$ - d -wave Zeeman fields in the conventional square lattice model. Contour map of the spin splitting subtracting the down-spin energy from the up-spin energy is shown in the fourth column. In the fifth column, we show the resultant spatial structure of nonuniform superconductivity in a large field from our GL theory.

Model	Transfer integral (dispersion)	Anisotropic field \hat{H}_{mag}	Spin splitting	$Q \neq 0$ superconductivity
(a) two-sublattice tetragonal		$-h\hat{\tau}_z \otimes \hat{\sigma}_z$ [Eq. (5)]		Phase-modulated (FF) [Sec. III B, Fig. 4]
(b) continuum		$-\sqrt{2}h(k_{nx}^2 - k_{ny}^2)\hat{\sigma}_z$ [Eq. (10)]		Amplitude-modulated (LO or bidirectional PDW) [Sec. III C 2, Fig. 5(b)]
(c1) conventional square lattice ($1k$ - d -wave)		$-h(\cos k'_x - \cos k'_y)\hat{\sigma}_z$ [Eq. (15)]		Amplitude-modulated (LO or bidirectional PDW) [Sec. III D, Fig. 6(a)]
(c2) conventional square lattice ($2k$ - d -wave)		$-h[\cos(2k'_x) - \cos(2k'_y)]\hat{\sigma}_z$ [Eq. (16)]		Phase-modulated (FF) [Sec. III D, Fig. 6(b)]

Here the unitary matrices representing the symmetry operations are defined by

$$\hat{U}_{C_{4z}} := \hat{\tau}_x \otimes \exp\left(-i\frac{\pi}{4}\hat{\sigma}_z\right), \quad (8a)$$

$$\hat{U}_{M_x} := \hat{\tau}_x \otimes (-i\hat{\sigma}_x), \quad (8b)$$

$$\hat{U}_T := \hat{\tau}_0 \otimes i\hat{\sigma}_y. \quad (8c)$$

When the altermagnetic order is turned on, some of the symmetries (including time-reversal symmetry T) are broken, and the remaining symmetry operations are represented by $4'mm'$, which is a subgroup of $4mm1'$.

By diagonalizing the noninteracting Hamiltonian $\hat{H}_0(\mathbf{k})$, we obtain the energy band dispersion. Figures 1(a) and 1(b) show

the energy band structures for $h = 0$ and $h = 0.4$, respectively. When the molecular field h is finite, the spin splitting appears at general \mathbf{k} points, except along the $k_{x,y}$ axes and the BZ boundary [see also the fourth column in Table I(a)]. In the following discussions, we focus on a hole-doped case with the electron density $n = n_\uparrow + n_\downarrow$ per site being 0.85 since our previous study has indicated that the FFLO state is more likely in the hole-doped regime [25]. The green dashed lines in Figs. 1(a) and 1(b) show the Fermi level for $n = 0.85$.

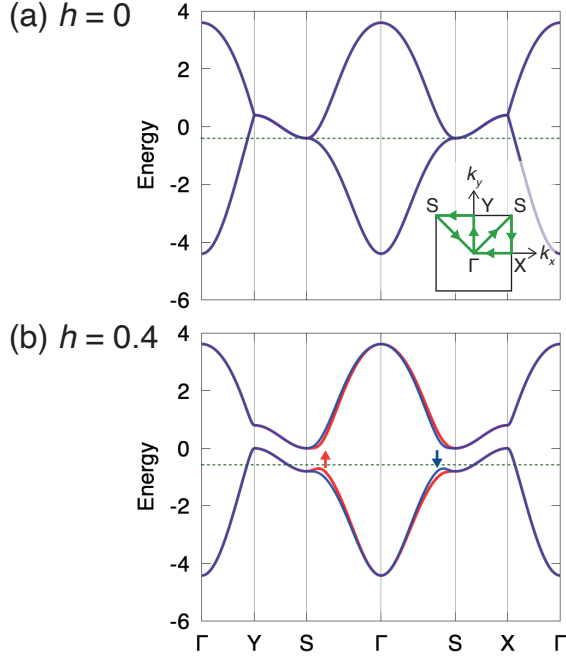


FIG. 1. Energy band structures for (a) $h = 0$ and (b) $h = 0.4$. Energy bands of up- and down-spin electrons are represented by the red and blue lines, respectively. The green dashed line represents the Fermi level for the electron density $n = 0.85$ per site. The inset in (a) shows the high-symmetry path in the 2D BZ. We use symbols (Γ , X, Y, S) of the primitive orthorhombic lattice since the fourfold rotation symmetry is broken in the altermagnetic state.

B. Continuum model

Next, we introduce the isotropic continuum model with the Zeeman field, as shown in Table I(b). Since this model does not contain the sublattice degree of freedom, the annihilation operator in Eq. (1) is now given by $\mathbf{C}_{\mathbf{k}} = [c_{\mathbf{k},\uparrow}, c_{\mathbf{k},\downarrow}]^T$, and the Hamiltonian is written as

$$\hat{H}_{\text{kin}}(\mathbf{k}) = \frac{k^2}{2m} \hat{\sigma}_0, \quad (9)$$

$$\hat{H}_{\text{mag}}(\mathbf{k}) = -h(\mathbf{k}_n) \hat{\sigma}_z, \quad (10)$$

where the kinetic term is a parabolic dispersion. The Zeeman field in Eq. (10) depends on the direction of the momentum $\mathbf{k}_n = \mathbf{k}/|\mathbf{k}|$. In Sec. III C, we discuss the GL theory for two types of the momentum dependence, namely, a uniform Zeeman field

$$h(\mathbf{k}_n) = h, \quad (11)$$

and a d -wave Zeeman field (cf. Refs. [26, 30–35])

$$h(\mathbf{k}_n) = \sqrt{2}h(k_{nx}^2 - k_{ny}^2), \quad (12)$$

with h being a magnitude of the magnetic order or magnetic field. Particularly in the d -wave Zeeman field (12), the energy dispersion exhibits anisotropic spin splitting resembling that in altermagnets, as shown in Table I(b).

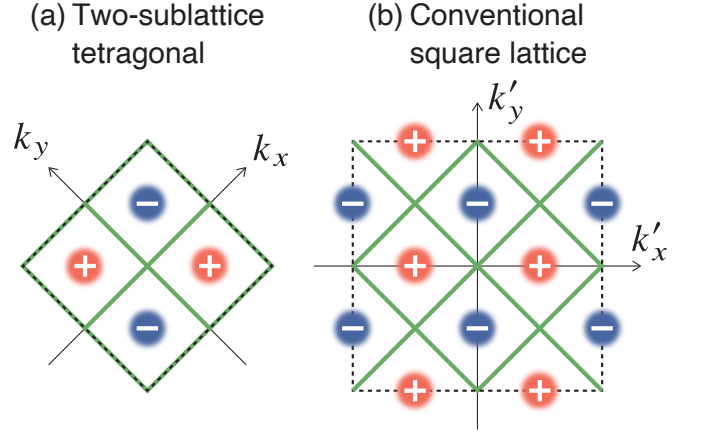


FIG. 2. The first BZs associated with the spin splitting structures in (a) the two-sublattice tetragonal model and (b) the conventional square lattice model with $2k$ - d -wave Zeeman field. In the altermagnetic state, energy dispersions have d -wave type spin splitting, which is illustrated by the plus and minus signs. Green lines represent the nodes, where the up- and down-spin bands are degenerate even in the presence of the magnetic order.

C. Conventional square lattice model

Finally, we introduce the conventional square lattice model with an anisotropic Zeeman term [Table I(c)]. In the two-sublattice tetragonal model (Sec. II A), the d -wave type spin splitting emerges when the anisotropic third-nearest-neighbor hopping t_2 and the molecular field h alternating on the two sublattices are finite. Here, to mimic the spin splitting, we consider a momentum-dependent Zeeman field. The annihilation operator in Eq. (1) is given by $\mathbf{C}_{\mathbf{k}'} = [c_{\mathbf{k}',\uparrow}, c_{\mathbf{k}',\downarrow}]^T$, and the Hamiltonian is

$$\hat{H}_{\text{kin}}(\mathbf{k}') = -2t_1(\cos k'_x + \cos k'_y) \hat{\sigma}_0 - 2t_2(\cos 2k'_x + \cos 2k'_y) \hat{\sigma}_0, \quad (13)$$

$$\hat{H}_{\text{mag}}(\mathbf{k}') = -h(\mathbf{k}') \hat{\sigma}_z, \quad (14)$$

which only have the spin degree of freedom described by the spin space Pauli matrices $\hat{\sigma}_j$. We use the primed momentum \mathbf{k}' to distinguish the momentum \mathbf{k} in the two-sublattice tetragonal model [Eqs. (4) and (5)], where the sublattice degree of freedom was described by the Pauli matrices $\hat{\tau}_i$. Considering the folding of the BZ, (k'_x, k'_y) is identified as $\frac{1}{2}(k_x - k_y, k_x + k_y)$ (see Fig. 2). The kinetic term (13) contains the transfer integral t_2 for all third-nearest neighbors, in contrast to the anisotropic t_2 in the two-sublattice tetragonal model [Eq. (4)].

Equation (14), which has the same form with Eq. (10) in the continuum model, represents the momentum-dependent Zeeman field. We consider two forms of $h(\mathbf{k}')$; the first one is given by

$$h(\mathbf{k}') = h(\cos k'_x - \cos k'_y), \quad (15)$$

which gives the d -wave type structure of spin splitting as shown in the fourth column in Table I(c1). While this form of $h(\mathbf{k}')$

was discussed in previous studies [27–29], strictly speaking, it generates a spin-split structure different from that in the two-sublattice tetragonal model, in which the nodes (green lines) are located at the zone boundaries $k_i = \pm\pi$ ($i = x, y$) as well as the interior $k_i = 0$ [see the fourth column in Table I(a)]. Therefore, here we introduce another form of $h(\mathbf{k}')$ with momentum doubling,

$$h(\mathbf{k}') = h[\cos(2k'_x) - \cos(2k'_y)]. \quad (16)$$

The splitting structure in the enlarged BZ of the conventional square lattice model with one sublattice is illustrated in the fourth column in Table I(c2), which reproduces the structure in the two-sublattice tetragonal model (see Fig. 2). To distinguish the two cases, we will refer to Eqs. (15) and (16) as the $1\mathbf{k}$ - and $2\mathbf{k}$ - d -wave Zeeman fields, respectively.

III. GINZBURG–LANDAU THEORY

In this section, to discuss the spatial structure of finite-momentum superconductivity in altermagnets, we construct the GL theory based on the microscopic Hamiltonian with superconducting instability. First, we show the general formalism of the GL theory in Sec. III A. Next, in Secs. III B–III D, we apply the theory to the three models that were introduced in Sec. II. The source codes used for the numerical calculations are available in Ref. [45].

A. Formalism

We here introduce the microscopic derivation of the GL theory [46–48]. Let us begin with the Hamiltonian using the superconducting MF approximation with an order parameter $\hat{\Delta}(\mathbf{x}, \mathbf{x}')$,

$$H_{\text{MF}} = H_0 + \frac{1}{2} \sum_{\mathbf{x}, \mathbf{x}'} \sum_{\zeta, \zeta'} \left[\Delta(\mathbf{x}, \mathbf{x}')_{\zeta, \zeta'} c_{\mathbf{x}, \zeta}^\dagger c_{\mathbf{x}', \zeta'}^\dagger + \text{H.c.} \right], \quad (17)$$

where \mathbf{x} and \mathbf{x}' represent real-space coordinates, and we label the internal degrees of freedom with ζ . We perform Fourier transformation with respect to the relative coordinate $\mathbf{r} = \mathbf{x} - \mathbf{x}'$:

$$\hat{\Delta}(\mathbf{x}, \mathbf{x}') = \frac{1}{N} \sum_{\mathbf{k}} e^{i\mathbf{k}\cdot\mathbf{r}} \hat{\Delta}(\mathbf{R}, \mathbf{k}), \quad (18a)$$

$$\hat{\Delta}(\mathbf{R}, \mathbf{k}) = \sum_{\mathbf{r}} e^{-i\mathbf{k}\cdot\mathbf{r}} \hat{\Delta}\left(\mathbf{R} + \frac{\mathbf{r}}{2}, \mathbf{R} - \frac{\mathbf{r}}{2}\right), \quad (18b)$$

where $\mathbf{R} = (\mathbf{x} + \mathbf{x}')/2$ is the COM coordinate and N is the number of unit cells. Equation (18b) is called the Wigner representation of the order parameter matrix [49]. We here consider a separable form $\hat{\Delta}(\mathbf{R}, \mathbf{k}) = \eta(\mathbf{R})\hat{\phi}(\mathbf{k})$ of the order parameter, where the magnitude $\eta(\mathbf{R})$ satisfies the MF equation

$$\eta(\mathbf{R}) = -\frac{TV}{N} \sum_{\mathbf{k}} \text{tr} [\hat{\phi}(\mathbf{k})^\dagger \hat{F}(\mathbf{R}, \mathbf{k}; \omega_n)], \quad (19)$$

with an effective interaction $V > 0$. We use the fermionic Matsubara frequency $\omega_n = (2n+1)\pi T$ at temperature T and the abbreviation $\sum_{\mathbf{k}} = \sum_{\omega_n} \sum_{\mathbf{k}}$. $\hat{\phi}(\mathbf{k})$ provides the matrix basis of the order parameter satisfying $\hat{\phi}(\mathbf{k}) = -\hat{\phi}(-\mathbf{k})^\top$, where the overall factor is chosen so that the normalization condition

$$\frac{1}{N} \sum_{\mathbf{k}} \text{tr} [\hat{\phi}(\mathbf{k})^\dagger \hat{\phi}(\mathbf{k})] = (\text{spin degree of freedom}) = 2 \quad (20)$$

is satisfied. The Wigner representation $F(\mathbf{R}, \mathbf{k}; \omega_n)_{\zeta, \zeta'}$ is obtained by Fourier transformation of the anomalous Green's function $F(\mathbf{x}, \mathbf{x}'; \tau)_{\zeta, \zeta'} = -\langle T_\tau c_{\mathbf{x}, \zeta}(\tau) c_{\mathbf{x}', \zeta'} \rangle$ with respect to the relative coordinate \mathbf{r} and the imaginary time τ :

$$\hat{F}(\mathbf{R}, \mathbf{k}; \omega_n) = \sum_{\mathbf{r}} e^{-i\mathbf{k}\cdot\mathbf{r}} \int_0^\beta d\tau e^{i\omega_n\tau} \hat{F}\left(\mathbf{R} + \frac{\mathbf{r}}{2}, \mathbf{R} - \frac{\mathbf{r}}{2}; \tau\right). \quad (21)$$

Next, we derive the GL equation and free energy. In the following, we assume that the magnitude of the order parameter $\eta(\mathbf{R})$ is sufficiently small and slowly varies with respect to \mathbf{R} . We expand the MF equation (19) with respect to η and its spatial derivative with the use of the Gor'kov equations,

$$\begin{aligned} \hat{G}(\mathbf{x}, \mathbf{x}'; \omega_n) &= \hat{G}_0(\mathbf{x}, \mathbf{x}'; \omega_n) \\ &\quad - \sum_{\mathbf{x}_1, \mathbf{x}_2} \hat{G}_0(\mathbf{x}, \mathbf{x}_1; \omega_n) \hat{\Delta}(\mathbf{x}_1, \mathbf{x}_2) \hat{F}(\mathbf{x}_2, \mathbf{x}'; \omega_n)^*, \end{aligned} \quad (22a)$$

$$\hat{F}(\mathbf{x}, \mathbf{x}'; \omega_n) = - \sum_{\mathbf{x}_1, \mathbf{x}_2} \hat{G}_0(\mathbf{x}, \mathbf{x}_1; \omega_n) \hat{\Delta}(\mathbf{x}_1, \mathbf{x}_2) \hat{G}(\mathbf{x}_2, \mathbf{x}'; \omega_n)^*, \quad (22b)$$

where $G(\mathbf{x}, \mathbf{x}'; \omega_n)_{\zeta, \zeta'}$ is the Fourier component of the normal Green's function $G(\mathbf{x}, \mathbf{x}'; \tau)_{\zeta, \zeta'} = -\langle T_\tau c_{\mathbf{x}, \zeta}(\tau) c_{\mathbf{x}', \zeta'}^\dagger \rangle$, and \hat{G}_0 is the normal Green's function of free electrons. After some calculations, we obtain the GL equation,

$$\begin{aligned} \alpha\eta(\mathbf{R}) + 2\beta|\eta(\mathbf{R})|^2\eta(\mathbf{R}) - \kappa\nabla_{\mathbf{R}}^2\eta(\mathbf{R}) \\ + \delta\nabla_{\mathbf{R}}^4\eta(\mathbf{R}) + \delta'\partial_X^2\partial_Y^2\eta(\mathbf{R}) \\ + (\text{higher-order terms}) = 0, \end{aligned} \quad (23)$$

in tetragonal systems. For the detailed derivation, see Appendix B. This equation can be seen as a saddle point solution $\delta\mathcal{F}/\delta\eta^* = 0$ of the free energy functional $\mathcal{F}[\eta(\mathbf{R})] = \frac{1}{\mathcal{V}} \int d\mathbf{R} f(\mathbf{R})$ with \mathcal{V} being the volume of the system. The GL free energy density per unit cell is then defined by

$$f = \alpha|\eta|^2 + \beta|\eta|^4 + \kappa|\nabla\eta|^2 + \delta|\nabla^2\eta|^2 + \delta'|\partial_X\partial_Y\eta|^2, \quad (24)$$

up to the fourth order of η and spatial derivatives ∂_i (we omit the \mathbf{R} dependence for simplicity). The GL coefficients of the uniform terms are calculated as

$$\alpha = \frac{1}{V} - \frac{T}{N} \sum_{\mathbf{k}} \text{tr} [\hat{X}(\mathbf{k}, \mathbf{0}; \omega_n)], \quad (25)$$

$$\beta = \frac{T}{2N} \sum_{\mathbf{k}} \text{tr} [\hat{X}(\mathbf{k}, \mathbf{0}; \omega_n)^2], \quad (26)$$

where we define

$$\hat{X}(\mathbf{k}, \mathbf{Q}; \omega_n) := \hat{\phi}(\mathbf{k})^\dagger \hat{G}_0(\mathbf{k}_+; \omega_n) \hat{\phi}(\mathbf{k}) \hat{G}_0(\mathbf{k}_-; \omega_n)^*, \quad (27)$$

with $\mathbf{k}_\pm = \pm \mathbf{k} + \mathbf{Q}$ and the noninteracting Green's function $\hat{G}_0(\mathbf{k}; \omega_n) = [(i\omega_n + \mu)\mathbf{1} - \hat{H}_0(\mathbf{k})]^{-1}$ for the chemical potential μ . The coefficients of the gradient terms are given by

$$\kappa = -c_{XX}^{(2)} = -c_{YY}^{(2)}, \quad (28)$$

$$\delta = c_{XXXX}^{(2)} = c_{YYYY}^{(2)}, \quad (29)$$

$$\delta' = 6c_{XXYY}^{(2)} - 2c_{XXXX}^{(2)}, \quad (30)$$

where

$$c_{\mu_1 \dots \mu_n}^{(2)} := -\frac{1}{n!} \frac{T}{(2i)^n N} \times \sum_{\mathbf{k}} \frac{\partial^n}{\partial Q_{\mu_1} \dots \partial Q_{\mu_n}} \text{tr} [\hat{X}(\mathbf{k}, \mathbf{Q}; \omega_n)] \Big|_{\mathbf{Q}=0}. \quad (31)$$

Note that δ' corresponds to the anisotropic term allowed in the tetragonal system. In the formulation of Eqs. (25)–(26) and (28)–(30), we do not include the effect of vector potential since we consider cases without an external magnetic field.

Before showing the results analyzing the derived GL coefficients, let us briefly review how the GL theory provides the interpretation of the ‘usual’ FFLO state in a uniform Zeeman field [40, 41], on the basis of GL free energy in Eq. (24). Here let h be the magnitude of the uniform Zeeman field. When h is small, the superconducting transition temperature $T_c(h)$ is determined by the condition $\alpha = 0$ (see Fig. 3). Around the transition temperature, both β and κ are positive. Next, considering the higher magnetic field region along the transition line, β and κ change their sign to negative almost *simultaneously* (we can show that the sign changes exactly coincide in the isotropic continuum model; see Sec. III C). Because of the negative κ , a spatially modulated superconducting state with finite COM momentum is more stable than a uniform state. Assuming a *phase-modulated* FF state $\eta(\mathbf{R}) = \eta_0 e^{2i\mathbf{Q}\cdot\mathbf{R}}$, where η_0 is the solution of the self-consistent gap equation, the COM momentum \mathbf{Q} that minimizes the free energy is given by

$$2\mathbf{Q} = \begin{cases} \left(\pm\sqrt{\frac{-\kappa}{2\delta}}, 0 \right), \left(0, \pm\sqrt{\frac{-\kappa}{2\delta}} \right) & \delta' \geq 0, \\ \left(\pm\sqrt{\frac{-\kappa}{4\delta+\delta'}}, \pm\sqrt{\frac{-\kappa}{4\delta+\delta'}} \right) & \delta' < 0, \end{cases} \quad (32)$$

where we assume $\delta > 0$ and $4\delta + \delta' > 0$ (indeed, these inequalities are satisfied in our numerical calculations around the FFLO region presented in Sec. III B). At the optimal COM momentum, we obtain the free energy

$$\mathcal{F}_{\text{FF}} = \tilde{\alpha}|\eta_0|^2 + \beta|\eta_0|^4, \quad (33)$$

where we define the renormalized coefficient

$$\tilde{\alpha} := \begin{cases} \alpha - \frac{\kappa^2}{4\delta} & \delta' \geq 0, \\ \alpha - \frac{\kappa^2}{4\delta+\delta'} & \delta' < 0. \end{cases} \quad (34)$$

In an *amplitude-modulated* LO state $\eta(\mathbf{R}) = \sqrt{2}\eta_0 \cos(2\mathbf{Q}\cdot\mathbf{R})$, on the other hand, the free energy is calculated as

$$\mathcal{F}_{\text{LO}} = \tilde{\alpha}|\eta_0|^2 + \frac{3}{2}\beta|\eta_0|^4, \quad (35)$$

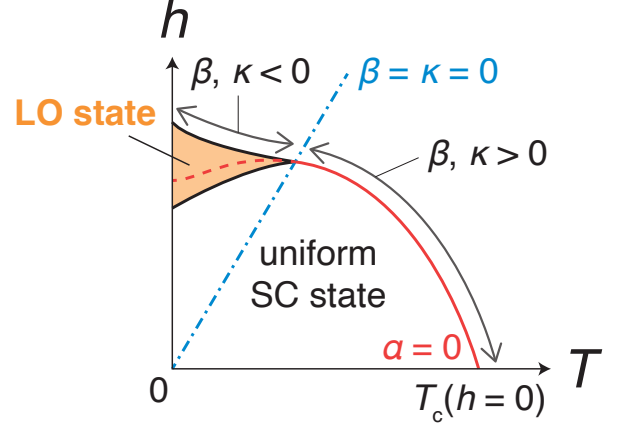


FIG. 3. Schematic phase diagram in a uniform Zeeman field h . The zeros of the GL coefficients α and β (κ) are depicted by red and blue lines, respectively. The amplitude-modulated LO state (orange shaded area) is stabilized in the high field region, where both β and κ are negative.

which is different from Eq. (33) in the fourth-order terms. Since β is negative when κ becomes negative as we mentioned, the LO state is more stabilized; this is the scenario for the case of the uniform Zeeman field. The key point here is the simultaneous sign change in β and κ . This situation is not always satisfied; for example, in Refs. [41, 50], it is proposed that the sign changes in β and κ deviate when the impurity effect is taken into account.

Note that the evaluation above is valid when κ is negative but close to zero; for large $|\kappa|$, namely a large COM momentum, the $O(|\eta_0|^4)$ terms in Eqs. (33) and (35) are corrected by terms with the fourth order in η and the second order in the derivatives [41]. In addition, when β is negative, we need take into account the sixth-order term in η , which is not included in Eq. (24), to discuss the transition temperature of the LO state. However, in this study we only consider the terms appearing in Eq. (24), which are the minimal set to identify whether a phase-modulated or an amplitude-modulated state is stabilized for a small negative κ .

B. Two-sublattice tetragonal model

In this subsection, we apply the GL theory to the two-sublattice tetragonal model, and also perform the MF calculations for finding the value of \mathbf{Q} . We show that the spatially nonuniform superconductivity coexisting with an altermagnetic order prefers the FF state, rather than the LO state that is realized in a uniform Zeeman field. Later, in the next subsections III C and III D, to look for the key ingredients giving rise to such a difference, comparisons will be made with other models with a momentum-dependent Zeeman field that has been used in most of previous studies working on FFLO superconductivity in an altermagnetic state [26, 27, 29–35] or a spin-triplet nematic state [36, 37].

1. Analyses of Ginzburg–Landau coefficients

Now let us move on to the main results, namely, the GL theory in the two-sublattice tetragonal model introduced in Sec. II A. Using Eqs. (25)–(26), (28)–(30), and (34), we computed the parameter dependence of the coefficients of the GL free energy, which determine the stability of different types of superconducting states. We here assume a d_{xy} -wave order parameter,

$$\hat{\phi}(\mathbf{k}) = \sqrt{2} \sin \frac{k_x}{2} \sin \frac{k_y}{2} \hat{\tau}_x \otimes i\hat{\sigma}_y, \quad (36)$$

which belongs to the B_2 irreducible representation (irrep) of the point group $4mm$. We confirmed that the B_2 order is the leading instability in many-body calculations of the on-site Hubbard model (Appendix A). For the calculations of Eqs. (25)–(26) and (28)–(30), we use the analytic form of the sum in Matsubara frequencies, and numerically computed the sum in \mathbf{k} using 512×512 meshes.

Figure 4 shows the zero lines of the GL coefficients in the parameter space of temperature (T) and altermagnetic molecular field strength (h). As in the case of a uniform Zeeman field reviewed above, the superconducting transition temperature for a small h is determined by the $\alpha = 0$ line (red open squares), around which both β and κ are positive. By increasing the altermagnetic field h , in contrast to the case of a uniform Zeeman field, along the $\alpha = 0$ line *only* κ changes its sign to negative (see the green dash-dotted line), whereas β remains positive. Therefore, *the phase-modulated FF state is stabilized in the high-altermagnetic-field regime*, according to Eqs. (33) and (35). This is a distinctive feature in altermagnetic systems, in clear contrast to the amplitude-modulated LO state in a uniform Zeeman field. We here note that the positive β around the transition temperature is consistent with previous quasiclassical calculations, which reported the absence of first-order transitions in high exchange fields [51].

2. Mean-field theory

To confirm the validity of our GL analysis, we evaluated the COM momentum of the Cooper pairs by self-consistent MF calculations. Assuming the FF state $\eta(\mathbf{R}) = \eta_0 e^{2i\mathbf{Q}\cdot\mathbf{R}}$ ($\eta_0 \in \mathbb{R}$), we introduce the Bogoliubov–de Gennes Hamiltonian within the MF approximation by

$$H_{\text{MF},\mathbf{Q}} = \sum_{\mathbf{k}} \Psi_{\mathbf{k},\mathbf{Q}}^\dagger \hat{H}_{\mathbf{Q}}(\mathbf{k}) \Psi_{\mathbf{k},\mathbf{Q}} + \text{const.}, \quad (37)$$

$$\hat{H}_{\mathbf{Q}}(\mathbf{k}) = \begin{bmatrix} \hat{H}_0(\mathbf{k}_+) & \eta_0 \hat{\phi}(\mathbf{k}) \\ \eta_0 \hat{\phi}(\mathbf{k})^\dagger & -\hat{H}_0(\mathbf{k}_-)^T \end{bmatrix}, \quad (38)$$

$$\Psi_{\mathbf{k},\mathbf{Q}} = [c_{\mathbf{k}_+,a\uparrow}, c_{\mathbf{k}_+,a\downarrow}, c_{\mathbf{k}_+,b\uparrow}, c_{\mathbf{k}_+,b\downarrow}, c_{\mathbf{k}_-,a\uparrow}^\dagger, c_{\mathbf{k}_-,a\downarrow}^\dagger, c_{\mathbf{k}_-,b\uparrow}^\dagger, c_{\mathbf{k}_-,b\downarrow}^\dagger]^T. \quad (39)$$

Then the grand potential in the superconducting state is given by

$$\Omega(\eta_0, \mathbf{Q}) = -\frac{T}{N} \sum_{\mathbf{k}} \text{tr} \left[\ln \left(1 + e^{-\hat{H}_{\mathbf{Q}}(\mathbf{k})/T} \right) \right] + \frac{\eta_0^2}{V}. \quad (40)$$

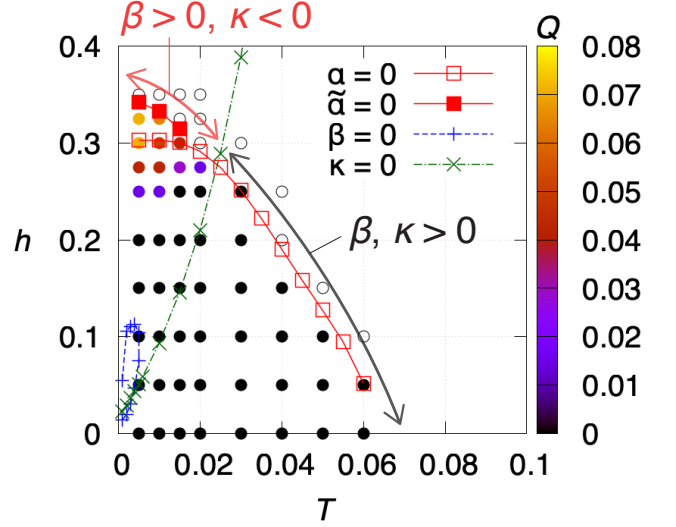


FIG. 4. Temperature (T) vs altermagnetic molecular field strength (h) phase diagram in the two-sublattice tetragonal model. The zeros of the GL coefficients $\tilde{\alpha}$, β , and κ are depicted by red solid, blue dashed, and green dash-dotted lines, respectively. The coefficient β is positive everywhere except in the narrow region enclosed by the blue dashed line. The filled (open) circles represent the superconducting (normal) state obtained by the MF theory, where the color of the filled circles indicates the magnitude of the optimal COM momentum $Q = |\mathbf{Q}|$. The effective interaction is set to $V = 0.35$.

The gap equation is represented as a derivative of the grand potential with respect to η_0 :

$$\frac{\partial}{\partial \eta_0} \Omega(\eta_0, \mathbf{Q}) = 0. \quad (41)$$

Let $\eta_0 = \eta_0(\mathbf{Q})$ be the solution of the self-consistent equation (41). The condensation energy for the FF superconductivity is thus written as

$$\mathcal{F}(\mathbf{Q}) = \Omega(\eta_0(\mathbf{Q}), \mathbf{Q}) - \Omega(0, \mathbf{Q}), \quad (42)$$

where $\Omega(0, \mathbf{Q}) = \Omega(0, \mathbf{0})$ holds.

We numerically solve the gap equation (41), and obtain the optimal COM momentum \mathbf{Q} that minimizes the condensation energy (42). The results of the MF analysis are illustrated in Fig. 4. The filled (open) circles represent the superconducting (normal) state, in which the condensation energy has a negative (positive) sign. The color of the filled circles indicates the magnitude of the optimal COM momentum \mathbf{Q} ; the black circles signify $\mathbf{Q} = \mathbf{0}$ (BCS state), while the other colored ones represent the FF state with finite momentum. Clearly, the FF state appears when the coefficient κ of the gradient term is negative, and its transition temperature corresponds to the $\tilde{\alpha} = 0$ line. Our calculations also indicate that \mathbf{Q} is parallel to the [11] direction. This is consistent with our GL analysis, which shows that δ' is always negative near the FF phase and results in $\mathbf{Q} \parallel [11]$ [see Eq. (32)].

C. Continuum model

We here investigate the GL coefficients in the continuum model introduced in Sec. II B. In the following discussions, we assume d -wave order parameter $\hat{\phi}(\mathbf{k}_n) = \sqrt{2}(k_{nx}^2 - k_{ny}^2)i\hat{\sigma}_y$; however, the results are not qualitatively altered in s -wave superconductors.

1. Uniform Zeeman field

First, we begin with the case in a uniform Zeeman field [Eq. (11)], as in the original theory of the FFLO state under a magnetic field [40, 41]. Following the procedure in Refs. [52–54], we can analytically evaluate the GL coefficients in Eqs. (25)–(28). Using the density of states ρ_F at the Fermi level, the coefficients are written as infinite series:

$$\alpha = \frac{1}{V} - \rho_F \sum_{n=0}^{\infty} (-1)^n S_{2n+1}(T) h^{2n}, \quad (43a)$$

$$\beta = \frac{12m^2}{k_F^2} \kappa = \frac{3\rho_F}{2} \sum_{n=1}^{\infty} (-1)^{n-1} \binom{2n}{2} S_{2n+1}(T) h^{2n-2}, \quad (43b)$$

where we define

$$S_l(T) := \pi T \sum_{\omega_n} \frac{1}{|\omega_n|^l} = \begin{cases} \log \frac{2e^{\gamma_E} E_c}{\pi T} & l = 1, \\ \frac{(2^l - 1)\zeta(l)}{(2\pi T)^{l-1}} & l \geq 2, \end{cases} \quad (44)$$

with $\gamma_E \approx 0.577$ and E_c being Euler's constant and the energy cutoff, respectively. For derivation of Eqs. (43a) and (43b), see Appendix C. Importantly, Eq. (43b) shows that β and κ are exactly proportional to each other with a constant factor $12m^2/k_F^2$. Therefore, the two coefficients changes their sign simultaneously and the amplitude-modulated superconducting state, such as the LO state, is stabilized in a large magnetic field, as explained in Sec. III A. Taking the first 100 terms of the infinite series in Eqs. (43a) and (43b), we compute the zeros of the GL coefficients, which are illustrated in Fig. 5(a). Note that, since the series are expanded by the powers of h/T , the calculation is not applicable to large h/T shown as the shaded area. Nevertheless, our calculations well reproduce the tricritical point $T = T^*$ at which all α , β , and κ becomes zero. Indeed, this point is located at $T^*/T_{c0} \approx 0.56$, which is consistent with previous studies [38–41, 55–57].

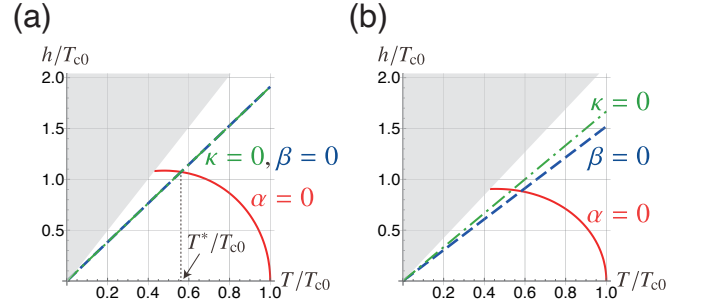


FIG. 5. Temperature (T) vs field strength (h) phase diagrams in the continuum model for the (a) uniform and (b) d -wave Zeeman fields. Both axes are scaled by the transition temperature at zero magnetic field T_{c0} . The $\alpha = 0$ lines are unreliable when h/T is large (dark shaded areas) since we truncate the infinite series after 100 terms.

2. d -wave Zeeman field

Next, let us consider the d -wave Zeeman field in Eq. (12). The GL coefficients are given by

$$\alpha = \frac{1}{V} - \rho_F \sum_{n=0}^{\infty} (-1)^n \frac{(2n+2)!}{2^{n+1}[(n+1)!]^2} S_{2n+1}(T) h^{2n}, \quad (45a)$$

$$\beta = \rho_F \sum_{n=1}^{\infty} (-1)^{n-1} \frac{(2n)!}{2^n(n!)^2} n \cdot \frac{4n^2 - 1}{n+1} S_{2n+1}(T) h^{2n-2}, \quad (45b)$$

$$\kappa = \frac{\rho_F k_F^2}{8m^2} \sum_{n=1}^{\infty} (-1)^{n-1} \frac{(2n)!}{2^n(n!)^2} n \times \left[(2n-1) - \frac{2n+1}{n+1} \left(\frac{h}{E_F} \right)^2 \right] S_{2n+1}(T) h^{2n-2}, \quad (45c)$$

where E_F is the Fermi energy; see Appendix C for the derivation. Since superconductors typically satisfy the weak-coupling condition $T_{c0} \ll E_F$, we assume that the d -wave field is much smaller than the Fermi energy, namely $h \ll E_F$, around the superconducting transition (for the analyses for strongly coupled superconductors, see Appendix C 1). Then the coefficient for the gradient term reduces to

$$\kappa = \frac{\rho_F k_F^2}{8m^2} \sum_{n=1}^{\infty} (-1)^{n-1} \frac{(2n)!}{2^n(n!)^2} n(2n-1) S_{2n+1}(T) h^{2n-2}, \quad (46)$$

where the summand is different from that in β [Eq. (45b)], in contrast to the uniform Zeeman case. Figure 5(b) shows the zeros of the GL coefficients in Eqs. (45a), (45b), and (46). Now, although the $\beta = 0$ and $\kappa = 0$ lines differ, we can see that the deviation is very small. In this model, therefore, the LO state is expected to occur even in the d -wave Zeeman field. This indicates that the FF state we obtained in Sec. III B cannot be explained by the Zeeman splitting in the continuum model. This result is consistent with Ref. [36], which proposed the stability of the LO state and bidirectional PDW state in a triplet α nematic phase.

D. Conventional square lattice model

Finally, let us apply the GL formalism to the conventional square lattice model introduced in Sec. II C. We here assume a $d_{x^2-y^2}$ -wave order parameter,

$$\hat{\phi}(\mathbf{k}') = (\cos k'_x - \cos k'_y)i\hat{\sigma}_y, \quad (47)$$

which corresponds to the d_{xy} -wave order in the two-sublattice tetragonal model [Eq. (36)]; recall that the coordinate axes in the \mathbf{k}' -space are rotated by $\pi/4$ radians from those in the \mathbf{k} -space (Fig. 2).

Considering the $1\mathbf{k}$ - d -wave Zeeman field [Eq. (15)], we numerically calculate the zeros of the GL coefficients [Eqs. (25)–(28)], which are shown in Fig. 6(a). One can see that the coefficients β and κ flip their signs almost simultaneously, and the phase diagram resembles the case of continuum model with the d -wave Zeeman field in Fig. 5(b). Therefore, again, the LO state is stable in the high field regime, in contrast to the FF state stabilized in the two-sublattice tetragonal model. We consider that the difference is caused by the form of the anisotropic Zeeman field, which does not reproduce the structure of spin splitting in the two-sublattice tetragonal model, as mentioned in Sec. II C.

Here, we propose an appropriate prescription of considering the $2\mathbf{k}$ - d -wave Zeeman field [Eq. (16)], consistent with spin splitting in the two-sublattice tetragonal model, which in fact shows the stable altermagnetism-induced FF state. Figure 6(b) shows the GL phase diagram calculated in the $2\mathbf{k}$ - d -wave Zeeman field. In this case, the phase diagram resembles much to the two-sublattice tetragonal model in Fig. 4, where only the coefficient κ changes its sign when $\alpha \approx 0$, whereas β is always positive around the transition temperature. This means that the FF state can emerge.

To summarize this section, our analyses indicate that *the multi-sublattice property is crucial for the occurrence of the altermagnetism-induced FF superconductivity*. Indeed, our two-sublattice tetragonal model [Eqs. (4) and (5)] contains two sublattices. Although the conventional square lattice model has no sublattice degree of freedom, the momentum doubling can effectively account for the BZ folding in the multi-sublattice system. In particular, since we consider the carrier density $n = 0.85$ near half-filling, the difference of spin-split structure sensitively affects the properties near the Fermi surfaces and therefore crucially influences the resultant superconducting state.

IV. SUMMARY AND DISCUSSION

In this study, we microscopically developed the GL theory in superconductors coexisting with an altermagnetic order, on the basis of three models: the two-sublattice tetragonal model, the continuum model, and the conventional square lattice model. In the first model, as the altermagnetic molecular field becomes large, the GL coefficient κ of the second-order gradient term changes sign from positive to negative, while the coefficient β of the fourth-order uniform term remains positive

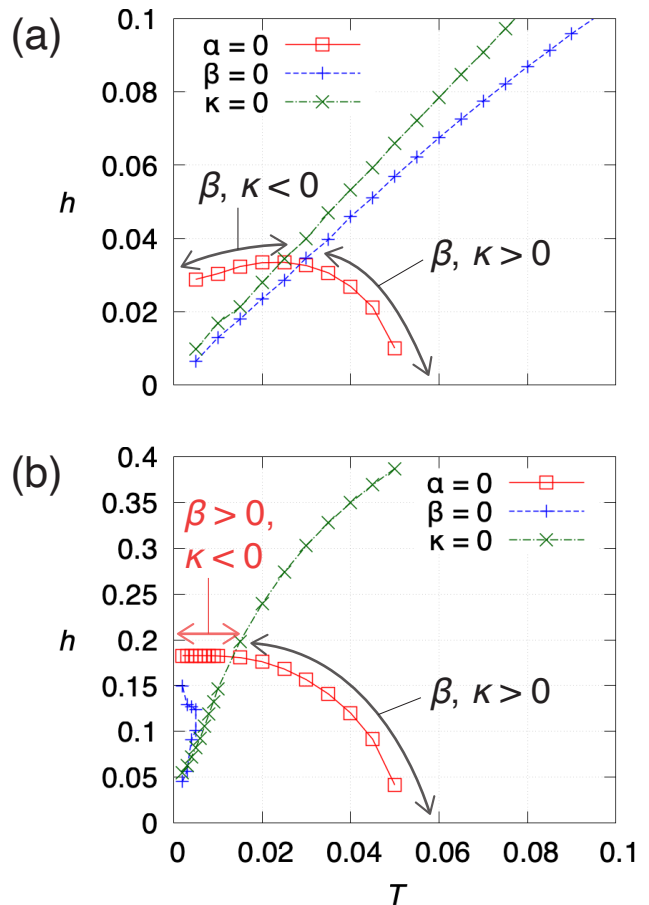


FIG. 6. T - h phase diagrams in the conventional square lattice model. We compute the GL coefficients in $1\mathbf{k}$ - d -wave [Eq. (15)] and $2\mathbf{k}$ - d -wave [(16)] Zeeman fields for (a) and (b), respectively. The effective interaction is set to $V = 0.35$.

around the superconducting transition temperature. As a consequence, a phase-modulated FF superconductivity is stabilized. This behavior is in drastic contrast with the well-known case of superconductivity in a uniform Zeeman field, where the amplitude-modulated LO state arises due to the simultaneous sign change of both β and κ .

We could identify the necessary ingredient for such exotic FF state to appear from the results of the other models: The continuum model and the conventional square lattice model in a $1\mathbf{k}$ - d -wave Zeeman field, which has often been used as the simplest representation of altermagnets in various studies [26, 27, 29–35], exhibit the stability of amplitude-modulated superconductivity. However, when we take into account the momentum doubling to the d -wave Zeeman field that reproduces the spin splitting structure in the two-sublattice tetragonal model, the FF state becomes more stable than the LO state even in the conventional square lattice model. Therefore, the multi-sublattice degree of freedom would be essential in realizing not only the altermagnetic state but also the exotic phase-modulated superconductivity.

Here we comment on the relevance of our theory to previous studies. The phase-modulated superconductivity with a single \mathbf{Q} has been proposed in the context of noncentrosymmetric superconductors [58–67], odd-parity magnetic multipoles [68–70], and anapole superconductivity [71, 72] (in the first context, it is also called as helical superconductivity). In addition, a recent theoretical study has suggested the emergence of an FF state in valley-polarized superconductors, which have a Fermi surface similar to that in f -wave altermagnets [73]. All the phase-modulated states discussed in these previous studies are attributed to odd-order terms concerning spatial derivatives, which can appear in the GL free energy by breaking the inversion and time-reversal symmetries [74]. In contrast, in our case the FF state can be stabilized even in the absence of odd orders; this situation is rather reminiscent of impurity effects under a uniform magnetic field [41, 50]. For the detection of the phase modulation in FF (helical) superconductivity, an interference experiment based on the Josephson effect has been proposed [63, 75, 76]. We believe that this method will also be effective in observing the FF state in altermagnets.

Our study shows that altermagnets constitute a novel and effective platform for phase-modulated FF superconductivity in the absence of an external magnetic field. A key ingredient for this exotic state is the multi-sublattice degree of freedom. As a future direction, cluster multipole systems, which includes altermagnets, are unexplored and interesting platforms to realize exotic quantum phenomena.

ACKNOWLEDGMENTS

The authors are grateful to Taira Kawamura, Yusuke Kato, Akito Daido, and Taisei Kitamura for valuable comments. This work was supported by Japan Society for the Promotion of Science (JSPS) KAKENHI Grants No. JP25H02113, No. JP23K03333, No. JP23K13056, No. JP23H01129, and No. JP23H04047. Some computations in this work were done using the facilities of the Supercomputer Center, the Institute for Solid State Physics, the University of Tokyo.

Appendix A: Eliashberg theory based on Hubbard model

For the analyses of the two-sublattice tetragonal model in the main text, we assume the d_{xy} -wave superconducting order belonging to the B_2 irrep [Eq. (36)] within the MF approximation. Here, we demonstrate that this d_{xy} -wave superconducting state is indeed the leading instability and the FFLO state can be stabilized on the basis of the Hubbard interaction and Eliashberg theory.

1. Formalism

In the following, we discuss the Hubbard Hamiltonian $H = H_0 + H_{\text{int}}^{(\text{Hub})}$, where the interaction term is given by

$$H_{\text{int}}^{(\text{Hub})} = U \sum_{\mathbf{R}} \sum_l n_{\mathbf{R},l\uparrow} n_{\mathbf{R},l\downarrow}, \quad (\text{A1})$$

with $U > 0$ being the onsite Coulomb repulsion. $n_{\mathbf{R},ls} = c_{\mathbf{R},ls}^\dagger c_{\mathbf{R},ls}$ is the electron-number operator.

To consider fluctuations of electric and magnetic multipoles, let us formulate the generalized susceptibility within the random-phase approximation. This is calculated as

$$\hat{\chi}(\mathbf{q}; \Omega_m) = [\hat{\mathbf{1}} - \hat{\chi}_0(\mathbf{q}; \Omega_m) \hat{U}^{(\text{Hub})}]^{-1} \hat{\chi}_0(\mathbf{q}; \Omega_m), \quad (\text{A2})$$

where $\Omega_m = 2m\pi T$ is the bosonic Matsubara frequency. The bare susceptibility χ_0 is defined by

$$\chi_0(q)_{\zeta_1\zeta_2, \zeta_3\zeta_4} = -\frac{T}{N} \sum_k G_0(k+q)_{\zeta_1, \zeta_3} G_0(k)_{\zeta_4, \zeta_2}, \quad (\text{A3})$$

where we use the abbreviations $k = (\mathbf{k}; \omega_n)$ and $q = (\mathbf{q}; \Omega_m)$. The matrix elements of the Hubbard interaction $\hat{U}^{(\text{Hub})}$ are defined by

$$U_{\zeta_1\zeta_2, \zeta_3\zeta_4}^{(\text{Hub})} = \delta_{l_1, l_2} \delta_{l_2, l_3} \delta_{l_3, l_4} U_{s_1 s_2, s_3 s_4}, \quad (\text{A4})$$

$$U_{s_1 s_2, s_3 s_4} = \begin{cases} U & (s_1 s_2, s_3 s_4) = (\uparrow\downarrow, \uparrow\downarrow) \text{ or } (\downarrow\uparrow, \downarrow\uparrow), \\ -U & (s_1 s_2, s_3 s_4) = (\uparrow\uparrow, \downarrow\downarrow) \text{ or } (\downarrow\downarrow, \uparrow\uparrow), \\ 0 & \text{otherwise.} \end{cases} \quad (\text{A5})$$

Next, we construct the linearized Eliashberg equation with finite COM momentum [25, 77]:

$$\lambda_{\mathbf{Q}} \Delta_{\mathbf{Q}}(k)_{\zeta, \zeta'} = \frac{T}{N} \sum_q \sum_{\zeta_1, \zeta_2} V^{(a)}(q)_{\zeta \zeta_1, \zeta_2 \zeta'} F_{\mathbf{Q}}(k-q)_{\zeta_1, \zeta_2}, \quad (\text{A6})$$

where $\hat{\Delta}_{\mathbf{Q}}(k)$ is the order parameter matrix, and the anomalous Green's function is given by

$$\hat{F}_{\mathbf{Q}}(k) = -\hat{G}_0(k) \hat{\Delta}_{\mathbf{Q}}(k) \hat{G}_0(-k + \mathbf{Q})^T, \quad (\text{A7})$$

with $\mathbf{Q} = (\mathbf{Q}; 0)$. Since we consider the multipole fluctuations as a glue of pairing, the interaction vertex are represented by using the generalized susceptibility (A2):

$$\hat{V}^{(a)}(q) = -\frac{1}{2} \hat{U}^{(\text{Hub})} - \hat{U}^{(\text{Hub})} \hat{\chi}(q) \hat{U}^{(\text{Hub})}. \quad (\text{A8})$$

In this finite-momentum Eliashberg theory, we can discuss the instability of the FF state with the COM momentum \mathbf{Q} for a given momentum \mathbf{Q} . The phase transition into the FF state takes place when the eigenvalue $\lambda_{\mathbf{Q}}$ in Eq. (A6) reaches unity.

2. Numerical results

Using the above formalism, let us investigate the possible superconducting order in an altermagnetic state. By using

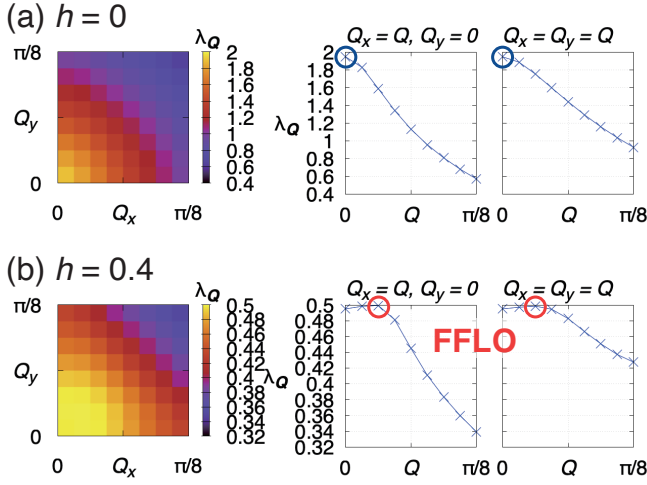


FIG. 7. The COM momentum dependence of the eigenvalue $\lambda_{\mathbf{Q}}$ of the Eliashberg equation (A6) for (a) $h = 0$ and (b) $h = 0.4$. The eigenvalue has peaks at finite momenta in (b).

the power method, we solve the linearized Eliashberg equation (A6). For a practical reason, we fix the temperature and seek the optimal combination of the COM momentum \mathbf{Q} and order parameter $\hat{\Delta}_{\mathbf{Q}}(k)$ that provides the largest eigenvalue $\lambda_{\mathbf{Q}}$. In the numerical study, we take 128×128 k -point meshes and about 90 Matsubara frequencies generated by SparseIR.jl package [78, 79] based on the intermediate representation [80] and the sparse sampling [81]. The temperature T and the energy cutoff ω_{\max} are set to $0.01t_1$ and $32t_1$, respectively. We consider the SC order parameter belonging to the four irreps of $4mm$: A_1 , A_2 , B_1 , and B_2 . Using $\tilde{\mathbf{k}} := \mathbf{k} - \mathbf{Q}/2$, the initial

functional form is chosen as

$$\hat{\Delta}_{\mathbf{Q}}^{(\text{init})}(k) \sim \begin{cases} \hat{\tau}_0 \otimes i\hat{\sigma}_y & \text{for } A_1, \\ (\cos \tilde{k}_x - \cos \tilde{k}_y)(\hat{\tau}_z \otimes i\hat{\sigma}_y) & \text{for } A_2, \\ (\cos \tilde{k}_x - \cos \tilde{k}_y)(\hat{\tau}_0 \otimes i\hat{\sigma}_y) & \text{for } B_1, \\ \sin \frac{\tilde{k}_x}{2} \sin \frac{\tilde{k}_y}{2} (\hat{\tau}_x \otimes i\hat{\sigma}_y) & \text{for } B_2. \end{cases} \quad (\text{A9})$$

We confirmed that the B_2 representation (d_{xy} -wave superconductivity) is the leading instability for superconductivity in our model for $0 \leq h \leq 0.4$.

Figure 7 shows the \mathbf{Q} dependence of the Eliashberg eigenvalue. In the paramagnetic state ($h = 0$), the eigenvalue has a single peak at zero momentum [Fig. 7(a)]. On the other hand, the maximum is located at finite \mathbf{Q} in the altermagnetic state with $h = 0.4$ [Fig. 7(b)]. This result indicates that the FFLO superconductivity is stabilized under the altermagnetic order.

Appendix B: Microscopic derivation of GL equation

We show the detailed derivation of the GL equation (23) from the Gor'kov equations (22). Here, we assume that the vector potential is absent, neglecting the orbital pair breaking effect due to an external magnetic field [82]. Therefore, the normal Green's function of free electrons is given by

$$\begin{aligned} \hat{G}_0(\mathbf{x}, \mathbf{x}'; \omega_n) &= \hat{G}_0(\mathbf{r}; \omega_n) \\ &= \frac{1}{N} \sum_{\mathbf{k}} e^{i\mathbf{k} \cdot \mathbf{r}} [(i\omega_n + \mu)\hat{\mathbf{1}} - \hat{H}_0(\mathbf{k})]^{-1}, \end{aligned} \quad (\text{B1})$$

which is a function of the relative coordinate $\mathbf{r} := \mathbf{x} - \mathbf{x}'$ because of the translation symmetry. Using the Wigner representation of the order parameter [Eq. (18b)], the Gor'kov equations (22) are rewritten as

$$\hat{G}(\mathbf{x}, \mathbf{x}'; \omega_n) = \hat{G}_0(\mathbf{r}; \omega_n) - \frac{1}{N} \sum_{\mathbf{r}_{12}, \mathbf{R}_{12}} \sum_{\mathbf{k}'} \eta(\mathbf{R}_{12}) e^{i\mathbf{k}' \cdot \mathbf{r}_{12}} \hat{G}_0\left(\mathbf{R} + \frac{\mathbf{r}}{2} - \mathbf{R}_{12} - \frac{\mathbf{r}_{12}}{2}; \omega_n\right) \hat{\phi}(\mathbf{k}') \hat{F}\left(\mathbf{R}_{12} - \frac{\mathbf{r}_{12}}{2}, \mathbf{R} - \frac{\mathbf{r}}{2}; \omega_n\right)^*, \quad (\text{B2a})$$

$$\hat{F}(\mathbf{x}, \mathbf{x}'; \omega_n) = -\frac{1}{N} \sum_{\mathbf{r}_{12}, \mathbf{R}_{12}} \sum_{\mathbf{k}'} \eta(\mathbf{R}_{12}) e^{i\mathbf{k}' \cdot \mathbf{r}_{12}} \hat{G}_0\left(\mathbf{R} + \frac{\mathbf{r}}{2} - \mathbf{R}_{12} - \frac{\mathbf{r}_{12}}{2}; \omega_n\right) \hat{\phi}(\mathbf{k}') \hat{G}\left(\mathbf{R}_{12} - \frac{\mathbf{r}_{12}}{2}, \mathbf{R} - \frac{\mathbf{r}}{2}; \omega_n\right)^*, \quad (\text{B2b})$$

where we define $\mathbf{R} := (\mathbf{x} + \mathbf{x}')/2$, $\mathbf{r}_{12} := \mathbf{x}_1 - \mathbf{x}_2$, and $\mathbf{R}_{12} := (\mathbf{x}_1 + \mathbf{x}_2)/2$. Using the above equations, we expand the right-hand side (RHS) of the MF equation (19) up to the third order of η :

$$\begin{aligned} [\text{RHS of Eq. (19)}] &= -\frac{TV}{N} \sum_{\omega_n} \sum_{\mathbf{r}} \sum_{\mathbf{k}} e^{-i\mathbf{k} \cdot \mathbf{r}} \text{tr} \left[\hat{\phi}(\mathbf{k})^\dagger \hat{F}\left(\mathbf{R} + \frac{\mathbf{r}}{2}, \mathbf{R} - \frac{\mathbf{r}}{2}; \omega_n\right) \right] \\ &= \frac{TV}{N^2} \sum_{\omega_n} \sum_{\mathbf{r}} \sum_{\mathbf{r}_{12}, \mathbf{R}_{12}} \sum_{\mathbf{k}, \mathbf{k}'} \eta(\mathbf{R}_{12}) e^{-i\mathbf{k} \cdot \mathbf{r} + i\mathbf{k}' \cdot \mathbf{r}_{12}} \\ &\quad \times \text{tr} \left[\hat{\phi}(\mathbf{k})^\dagger \hat{G}_0\left(\mathbf{R} + \frac{\mathbf{r}}{2} - \mathbf{R}_{12} - \frac{\mathbf{r}_{12}}{2}; \omega_n\right) \hat{\phi}(\mathbf{k}') \hat{G}\left(\mathbf{R}_{12} - \frac{\mathbf{r}_{12}}{2}, \mathbf{R} - \frac{\mathbf{r}}{2}; \omega_n\right)^* \right] \end{aligned}$$

$$\begin{aligned}
&= \frac{TV}{N^2} \sum_{\omega_n} \sum_{\mathbf{r}} \sum_{\mathbf{r}_{12}, \mathbf{R}_{12}} \sum_{\mathbf{k}, \mathbf{k}'} \eta(\mathbf{R}_{12}) e^{-i\mathbf{k} \cdot \mathbf{r} + i\mathbf{k}' \cdot \mathbf{r}_{12}} \\
&\quad \times \text{tr} \left[\hat{\phi}(\mathbf{k})^\dagger \hat{G}_0 \left(\mathbf{R} + \frac{\mathbf{r}}{2} - \mathbf{R}_{12} - \frac{\mathbf{r}_{12}}{2}; \omega_n \right) \hat{\phi}(\mathbf{k}') \hat{G}_0 \left(\mathbf{R}_{12} - \frac{\mathbf{r}_{12}}{2} - \mathbf{R} + \frac{\mathbf{r}}{2}; \omega_n \right)^* \right] \\
&- \frac{TV}{N^3} \sum_{\omega_n} \sum_{\mathbf{r}} \sum_{\mathbf{r}_{12}, \mathbf{R}_{12}} \sum_{\mathbf{r}_{34}, \mathbf{R}_{34}} \sum_{\mathbf{k}, \mathbf{k}', \mathbf{k}''} \eta(\mathbf{R}_{12}) \eta(\mathbf{R}_{34})^* e^{-i\mathbf{k} \cdot \mathbf{r} + i\mathbf{k}' \cdot \mathbf{r}_{12} - i\mathbf{k}'' \cdot \mathbf{r}_{34}} \\
&\quad \times \text{tr} \left[\hat{\phi}(\mathbf{k})^\dagger \hat{G}_0 \left(\mathbf{R} + \frac{\mathbf{r}}{2} - \mathbf{R}_{12} - \frac{\mathbf{r}_{12}}{2}; \omega_n \right) \hat{\phi}(\mathbf{k}') \hat{G}_0 \left(\mathbf{R}_{12} - \frac{\mathbf{r}_{12}}{2} - \mathbf{R}_{34} - \frac{\mathbf{r}_{34}}{2}; \omega_n \right)^* \right. \\
&\quad \left. \times \hat{\phi}(\mathbf{k}'')^* \hat{F} \left(\mathbf{R}_{34} - \frac{\mathbf{r}_{34}}{2}, \mathbf{R} - \frac{\mathbf{r}}{2}; \omega_n \right) \right] \\
&\simeq \frac{TV}{N^2} \sum_{\omega_n} \sum_{\mathbf{r}} \sum_{\mathbf{r}_{12}, \mathbf{R}_{12}} \sum_{\mathbf{k}, \mathbf{k}'} \eta(\mathbf{R}_{12}) e^{-i\mathbf{k} \cdot \mathbf{r} + i\mathbf{k}' \cdot \mathbf{r}_{12}} \\
&\quad \times \text{tr} \left[\hat{\phi}(\mathbf{k})^\dagger \hat{G}_0 \left(\mathbf{R} + \frac{\mathbf{r}}{2} - \mathbf{R}_{12} - \frac{\mathbf{r}_{12}}{2}; \omega_n \right) \hat{\phi}(\mathbf{k}') \hat{G}_0 \left(\mathbf{R}_{12} - \frac{\mathbf{r}_{12}}{2} - \mathbf{R} + \frac{\mathbf{r}}{2}; \omega_n \right)^* \right] \\
&- \frac{TV}{N^4} \sum_{\omega_n} \sum_{\mathbf{r}} \sum_{\mathbf{r}_{12}, \mathbf{R}_{12}} \sum_{\mathbf{r}_{34}, \mathbf{R}_{34}} \sum_{\mathbf{r}_{56}, \mathbf{R}_{56}} \sum_{\mathbf{k}, \mathbf{k}', \mathbf{k}'', \mathbf{k}'''} \eta(\mathbf{R}_{12}) \eta(\mathbf{R}_{34})^* \eta(\mathbf{R}_{56}) e^{-i\mathbf{k} \cdot \mathbf{r} + i\mathbf{k}' \cdot \mathbf{r}_{12} + i\mathbf{k}'' \cdot \mathbf{r}_{34} + i\mathbf{k}''' \cdot \mathbf{r}_{56}} \\
&\quad \times \text{tr} \left[\hat{\phi}(\mathbf{k})^\dagger \hat{G}_0 \left(\mathbf{R} + \frac{\mathbf{r}}{2} - \mathbf{R}_{12} - \frac{\mathbf{r}_{12}}{2}; \omega_n \right) \hat{\phi}(\mathbf{k}') \hat{G}_0 \left(\mathbf{R}_{12} - \frac{\mathbf{r}_{12}}{2} - \mathbf{R}_{34} - \frac{\mathbf{r}_{34}}{2}; \omega_n \right)^* \right. \\
&\quad \left. \times \hat{\phi}(\mathbf{k}'')^\dagger \hat{G}_0 \left(\mathbf{R}_{34} - \frac{\mathbf{r}_{34}}{2} - \mathbf{R}_{56} - \frac{\mathbf{r}_{56}}{2}; \omega_n \right) \hat{\phi}(\mathbf{k}''') \hat{G}_0 \left(\mathbf{R}_{56} - \frac{\mathbf{r}_{56}}{2} - \mathbf{R} + \frac{\mathbf{r}}{2}; \omega_n \right)^* \right]. \quad (\text{B3})
\end{aligned}$$

In the second term of the final expression, we use the transformation $\mathbf{k}'' \rightarrow -\mathbf{k}''$ and replace \hat{G} with \hat{G}_0 as an approximation. Using Eq. (B1), the first term in Eq. (B3) is further calculated as

$$\begin{aligned}
[\text{The first term in Eq. (B3)}] &= \frac{TV}{N^2} \sum_{\omega_n} \sum_{\mathbf{r}} \sum_{\mathbf{r}_{12}, \mathbf{R}_{12}} \sum_{\mathbf{k}, \mathbf{k}'} \eta(\mathbf{R}_{12}) e^{-i\mathbf{k} \cdot \mathbf{r} + i\mathbf{k}' \cdot \mathbf{r}_{12}} \\
&\quad \times \frac{1}{N^2} \sum_{\mathbf{k}_1, \mathbf{k}_2} e^{i\mathbf{k}_1 \cdot (\mathbf{R} + \frac{\mathbf{r}}{2} - \mathbf{R}_{12} - \frac{\mathbf{r}_{12}}{2})} e^{-i\mathbf{k}_2 \cdot (\mathbf{R}_{12} - \frac{\mathbf{r}_{12}}{2} - \mathbf{R} + \frac{\mathbf{r}}{2})} \text{tr} \left[\hat{\phi}(\mathbf{k})^\dagger \hat{G}_0(\mathbf{k}_1; \omega_n) \hat{\phi}(\mathbf{k}') \hat{G}_0(\mathbf{k}_2; \omega_n)^* \right] \\
&= \frac{TV}{N^2} \sum_{\omega_n} \sum_{\mathbf{k}, \mathbf{Q}} \sum_{\mathbf{R}_{12}} \frac{e^{-2i\mathbf{Q} \cdot (\mathbf{R}_{12} - \mathbf{R})} \eta(\mathbf{R}_{12})}{\text{tr} [\hat{X}(\mathbf{k}, \mathbf{Q}; \omega_n)]}. \quad (\text{B4})
\end{aligned}$$

Defining $\bar{\mathbf{R}} := \mathbf{R}_{12} - \mathbf{R}$, we expand $\eta(\mathbf{R}_{12}) = \eta(\mathbf{R} + \bar{\mathbf{R}})$ around \mathbf{R} . Then the underlined part is given by

$$\begin{aligned}
e^{-2i\mathbf{Q} \cdot \bar{\mathbf{R}}} \eta(\mathbf{R} + \bar{\mathbf{R}}) &= e^{-2i\mathbf{Q} \cdot \bar{\mathbf{R}}} \sum_{n=0}^{\infty} \frac{1}{n!} (\bar{\mathbf{R}} \cdot \nabla_{\mathbf{R}'})^n \eta(\mathbf{R}') \Big|_{\mathbf{R}'=\mathbf{R}} \\
&= e^{-2i\mathbf{Q} \cdot \bar{\mathbf{R}}} \eta(\mathbf{R}) + \sum_{n=1}^{\infty} \frac{1}{n!} \left(\frac{-1}{2i} \right)^n \sum_{\mu_1, \dots, \mu_n} \frac{\partial^n e^{-2i\mathbf{Q} \cdot \bar{\mathbf{R}}}}{\partial Q_{\mu_1} \cdots \partial Q_{\mu_n}} \cdot \frac{\partial^n \eta(\mathbf{R})}{\partial R_{\mu_1} \cdots \partial R_{\mu_n}}. \quad (\text{B5})
\end{aligned}$$

Assuming the slowly varying of the order parameter in the real space, we take the expansion up to the fourth order with respect to the derivative $\nabla_{\mathbf{R}}$. Then we obtain

$$\begin{aligned}
[\text{The first term in Eq. (B3)}] &\simeq \frac{TV}{N^2} \eta(\mathbf{R}) \sum_{\omega_n} \sum_{\mathbf{k}, \mathbf{Q}} \sum_{\bar{\mathbf{R}}} e^{-2i\mathbf{Q} \cdot \bar{\mathbf{R}}} \text{tr} [\hat{X}(\mathbf{k}, \mathbf{Q}; \omega_n)] \\
&\quad + \frac{TV}{N^2} \sum_{n=1}^4 \frac{1}{n!} \left(\frac{-1}{2i} \right)^n \sum_{\mu_1, \dots, \mu_n} \frac{\partial^n \eta(\mathbf{R})}{\partial R_{\mu_1} \cdots \partial R_{\mu_n}} \sum_{\omega_n} \sum_{\mathbf{k}, \mathbf{Q}} \sum_{\bar{\mathbf{R}}} \frac{\partial^n e^{-2i\mathbf{Q} \cdot \bar{\mathbf{R}}}}{\partial Q_{\mu_1} \cdots \partial Q_{\mu_n}} \cdot \text{tr} [\hat{X}(\mathbf{k}, \mathbf{Q}; \omega_n)] \\
&= \frac{TV}{N} \eta(\mathbf{R}) \sum_{\omega_n} \sum_{\mathbf{k}} \text{tr} [\hat{X}(\mathbf{k}, \mathbf{0}; \omega_n)] \\
&\quad + \frac{TV}{N} \sum_{n=1}^4 \frac{1}{n! (2i)^n} \sum_{\mu_1, \dots, \mu_n} \frac{\partial^n \eta(\mathbf{R})}{\partial R_{\mu_1} \cdots \partial R_{\mu_n}} \sum_{\omega_n} \sum_{\mathbf{k}} \frac{\partial^n}{\partial Q_{\mu_1} \cdots \partial Q_{\mu_n}} \text{tr} [\hat{X}(\mathbf{k}, \mathbf{Q}; \omega_n)] \Big|_{\mathbf{Q}=\mathbf{0}} \\
&= (1 - V\alpha) \eta(\mathbf{R}) - V \sum_{n=1}^4 \sum_{\mu_1, \dots, \mu_n} c_{\mu_1 \dots \mu_n}^{(2)} \frac{\partial^n \eta(\mathbf{R})}{\partial R_{\mu_1} \cdots \partial R_{\mu_n}}, \quad (\text{B6})
\end{aligned}$$

where we use Eqs. (25) and (31). On the other hand, the third-order term in η is given by

$$[\text{The second term in Eq. (B3)}] \simeq -\frac{TV}{N} |\eta(\mathbf{R})|^2 \eta(\mathbf{R}) \sum_{\omega_n} \sum_{\mathbf{k}} \text{tr} [\hat{X}(\mathbf{k}, \mathbf{0}; \omega_n)^2] = -2V\beta |\eta(\mathbf{R})|^2 \eta(\mathbf{R}), \quad (\text{B7})$$

where we neglect the spatial derivative and use Eq. (26). Substituting Eqs. (B6) and (B7) into the MF equation (19), we finally get the GL equation:

$$\begin{aligned} \eta(\mathbf{R}) &= (1 - V\alpha)\eta(\mathbf{R}) - 2V\beta |\eta(\mathbf{R})|^2 \eta(\mathbf{R}) - V \sum_{n=1}^4 \sum_{\mu_1, \dots, \mu_n} c_{\mu_1 \dots \mu_n}^{(2)} \frac{\partial^n \eta(\mathbf{R})}{\partial R_{\mu_1} \dots \partial R_{\mu_n}}, \\ \therefore \alpha \eta(\mathbf{R}) + 2\beta |\eta(\mathbf{R})|^2 \eta(\mathbf{R}) + \sum_{n=1}^4 \sum_{\mu_1, \dots, \mu_n} c_{\mu_1 \dots \mu_n}^{(2)} \frac{\partial^n \eta(\mathbf{R})}{\partial R_{\mu_1} \dots \partial R_{\mu_n}} &= 0. \end{aligned} \quad (\text{B8})$$

Imposing the symmetry of tetragonal systems on this equation, we can reproduce Eq. (23) in the main text.

Appendix C: GL coefficients in a continuum model

Following Refs. [52–54], we derive the GL coefficients of a continuum model in a Zeeman field [Eqs. (43) and (45)]. For the Hamiltonian in Eqs. (9) and (10), the Green's function of free electrons is given by

$$G_0(\mathbf{k}; \omega_n)_{s,s'} = \frac{\delta_{s,s'}}{i\omega_n - \xi(\mathbf{k}) + (-1)^s h(\mathbf{k})}, \quad (\text{C1})$$

where $\xi(\mathbf{k}) = \frac{k^2}{2m} - \mu$. Using this Green's function, we calculate the coefficients α , β , and κ [Eqs. (25)–(26) and (28)] by replacing the summation $\frac{1}{N} \sum_{\mathbf{k}}$ with an integral $\frac{1}{(2\pi)^2} \int d\mathbf{k}$. For the analytical calculations in the following, we will refer to some useful formulas, which are summarized at the end of this Appendix (Sec. C 2).

First, to discuss α and κ , let us consider the following integral,

$$I(\mathbf{Q}) := T \sum_{\omega_n} \int \frac{d\mathbf{k}}{(2\pi)^2} \text{tr} [\hat{X}(\mathbf{k}, \mathbf{Q}; \omega_n)], \quad (\text{C2})$$

whose expansion with respect to \mathbf{Q} includes the two coefficients:

$$I(\mathbf{Q}) = \left(\frac{1}{V} - \alpha \right) Q^0 - 4\kappa Q^2 + \mathcal{O}(Q^4). \quad (\text{C3})$$

Noting that $\xi(\mathbf{k})$ and $h(\mathbf{k})$ are even in \mathbf{k} , and using the $d_{x^2-y^2}$ -wave order parameter $\hat{\phi}(\mathbf{k}_n) = \sqrt{2}(k_{nx}^2 - k_{ny}^2) i\hat{\sigma}_y$, we calculate $I(\mathbf{Q})$ as

$$\begin{aligned} I(\mathbf{Q}) &= T \sum_s \sum_{\omega_n} \int \frac{d\mathbf{k}}{(2\pi)^2} \frac{2(k_{nx}^2 - k_{ny}^2)^2}{[i\omega_n - \xi(\mathbf{k} + \mathbf{Q}) + (-1)^s h(\mathbf{k} + \mathbf{Q})] [-i\omega_n - \xi(\mathbf{k} - \mathbf{Q}) - (-1)^s h(\mathbf{k} - \mathbf{Q})]} \\ &\simeq T \sum_s \sum_{\omega_n} \int \frac{d\mathbf{k}}{(2\pi)^2} \frac{2(k_{nx}^2 - k_{ny}^2)^2}{[i\omega_n - \xi(\mathbf{k}) - \mathbf{v}(\mathbf{k}) \cdot \mathbf{Q} + (-1)^s h(\mathbf{k} + \mathbf{Q})] [-i\omega_n - \xi(\mathbf{k}) + \mathbf{v}(\mathbf{k}) \cdot \mathbf{Q} - (-1)^s h(\mathbf{k} - \mathbf{Q})]} \\ &\simeq \rho_F T \sum_s \sum_{\omega_n} \int_{-\infty}^{\infty} d\xi \left\langle \frac{\cos^2(2\theta_{\mathbf{k}})}{[\xi - i\omega_n + \mathbf{v}(\mathbf{k}) \cdot \mathbf{Q} - (-1)^s h(\mathbf{k} + \mathbf{Q})] [\xi + i\omega_n - \mathbf{v}(\mathbf{k}) \cdot \mathbf{Q} + (-1)^s h(\mathbf{k} - \mathbf{Q})]} \right\rangle_{\text{FS}}, \end{aligned} \quad (\text{C4})$$

where $\mathbf{v}(\mathbf{k}) := \nabla_{\mathbf{k}} \xi(\mathbf{k}) = \mathbf{k}/m$ is the velocity. In the last line, we used the approximation

$$2 \int \frac{d\mathbf{k}}{(2\pi)^2} (\cdot) \simeq \rho_F \int_{-\infty}^{\infty} d\xi (\cdot)_{\text{FS}}, \quad (\text{C5})$$

$$\langle f(\mathbf{k}) \rangle_{\text{FS}} := \int_0^{2\pi} \frac{d\theta_{\mathbf{k}}}{2\pi} f(k_F \cos \theta_{\mathbf{k}}, k_F \sin \theta_{\mathbf{k}}), \quad (\text{C6})$$

where the angular average is taken over the undistorted Fermi surface with the Fermi momentum k_F . Using the for-

mula (C13), Equation (C4) is reduced to

$$\begin{aligned} I(\mathbf{Q}) &= \rho_F \pi T \sum_s \sum_{\omega_n} \left\langle \frac{\cos^2(2\theta_{\mathbf{k}})}{|\omega_n| + i\Omega_s(\mathbf{k}, \mathbf{Q}) \text{sgn}(\omega_n)} \right\rangle_{\text{FS}} \\ &= \rho_F \pi T \sum_s \sum_{\omega_n} \sum_{l=0}^{\infty} (-1)^l \left\langle \cos^2(2\theta_{\mathbf{k}}) \frac{\Omega_s(\mathbf{k}, \mathbf{Q})^{2l}}{|\omega_n|^{2l+1}} \right\rangle_{\text{FS}} \\ &= \rho_F \sum_s \sum_{l=0}^{\infty} (-1)^l S_{2l+1}(T) \langle \cos^2(2\theta_{\mathbf{k}}) \Omega_s(\mathbf{k}, \mathbf{Q})^{2l} \rangle_{\text{FS}}, \end{aligned} \quad (\text{C7})$$

where we define

$$\begin{aligned}\Omega_s(\mathbf{k}, \mathbf{Q}) &:= \mathbf{v}(\mathbf{k}) \cdot \mathbf{Q} - \frac{(-1)^s}{2} [h(\mathbf{k} + \mathbf{Q}) + h(\mathbf{k} - \mathbf{Q})] \\ &= (-1)^{s-1} h(\mathbf{k}) + \mathbf{v}(\mathbf{k}) \cdot \mathbf{Q} + \frac{(-1)^{s-1}}{2} (\mathbf{Q} \cdot \nabla_{\mathbf{k}})^2 h(\mathbf{k}) + \dots\end{aligned}\quad (\text{C8})$$

Then we expand $\sum_s \Omega_s(\mathbf{k}, \mathbf{Q})^{2l}$ ($l \geq 1$) with respect to \mathbf{Q} :

$$\begin{aligned}\sum_s \Omega_s(\mathbf{k}, \mathbf{Q})^{2l} &= 2h(\mathbf{k})^{2l} + 2 \cdot \binom{2l}{1} h(\mathbf{k})^{2l-1} (\mathbf{Q} \cdot \nabla_{\mathbf{k}})^2 h(\mathbf{k}) \\ &\quad + 2 \cdot \binom{2l}{2} h(\mathbf{k})^{2l-2} [\mathbf{v}(\mathbf{k}) \cdot \mathbf{Q}]^2 + \dots\end{aligned}\quad (\text{C9})$$

From Eqs. (C3), (C7), and (C9), therefore, the GL coefficients

α and κ are given by

$$\begin{aligned}\alpha &= \frac{1}{V} - 2\rho_{\text{F}} \sum_{l=0}^{\infty} (-1)^l S_{2l+1}(T) \langle \cos^2(2\theta_{\mathbf{k}}) h(\mathbf{k})^{2l} \rangle_{\text{FS}}, \\ \kappa &= \frac{\rho_{\text{F}} k_{\text{F}}^2}{2m^2} \sum_{l=1}^{\infty} (-1)^{l-1} \binom{2l}{2} S_{2l+1}(T) \left\langle \cos^2(2\theta_{\mathbf{k}}) \right. \\ &\quad \left. \times \left[\frac{2m^2 h(\mathbf{k})^{2l-1}}{(2l-1)k_{\text{F}}^2} (\hat{\mathbf{Q}} \cdot \nabla_{\mathbf{k}})^2 h(\mathbf{k}) + h(\mathbf{k})^{2l-2} (\mathbf{k}_n \cdot \hat{\mathbf{Q}})^2 \right] \right\rangle_{\text{FS}}.\end{aligned}\quad (\text{C10})$$

Using the formulas (C15)–(C17), one can reproduce Eqs. (43a) and (43b) for a uniform Zeeman field [$h(\mathbf{k}) = h$], and Eqs. (45a) and (45c) for a momentum-dependent Zeeman field [$h(\mathbf{k}) = \sqrt{2}h(k_{nx}^2 - k_{ny}^2) = \sqrt{2}h \cos(2\theta_{\mathbf{k}})$].

Next, the coefficient β is calculated in a similar way to $I(\mathbf{Q})$:

$$\begin{aligned}\beta &= \frac{T}{2} \sum_{\omega_n} \int \frac{d\mathbf{k}}{(2\pi)^2} \text{tr} [\hat{X}(\mathbf{k}, \mathbf{0}; \omega_n)^2] \\ &= T \sum_s \sum_{\omega_n} \int \frac{d\mathbf{k}}{(2\pi)^2} \frac{2(k_{nx}^2 - k_{ny}^2)^4}{[i\omega_n - \xi(\mathbf{k}) + (-1)^s h(\mathbf{k})]^2 [-i\omega_n - \xi(\mathbf{k}) - (-1)^s h(\mathbf{k})]^2} \\ &\simeq \rho_{\text{F}} T \sum_s \sum_{\omega_n} \int_{-\infty}^{\infty} d\xi \left\langle \frac{\cos^4(2\theta_{\mathbf{k}})}{[\xi - i\omega_n - (-1)^s h(\mathbf{k})]^2 [\xi + i\omega_n + (-1)^s h(\mathbf{k})]^2} \right\rangle_{\text{FS}} \\ &= \frac{\rho_{\text{F}}}{2} \pi T \sum_s \sum_{\omega_n} \left\langle \frac{\cos^4(2\theta_{\mathbf{k}})}{[|\omega_n| - i(-1)^s h(\mathbf{k}) \text{sgn}(\omega_n)]^3} \right\rangle_{\text{FS}} \\ &= \frac{\rho_{\text{F}}}{2} \pi T \sum_s \sum_{\omega_n} \sum_{l=1}^{\infty} (-1)^{l-1} \binom{2l}{2} \left\langle \cos^4(2\theta_{\mathbf{k}}) \frac{h(\mathbf{k})^{2l-2}}{|\omega_n|^{2l+1}} \right\rangle_{\text{FS}} \\ &= \rho_{\text{F}} \sum_{l=1}^{\infty} (-1)^{l-1} \binom{2l}{2} S_{2l+1}(T) \langle \cos^4(2\theta_{\mathbf{k}}) h(\mathbf{k})^{2l-2} \rangle_{\text{FS}},\end{aligned}\quad (\text{C12})$$

where we used the formula (C14). With the help of the formula (C15), this equation results in Eq. (43b) for a uniform Zeeman field, and Eq. (45b) for a $d_{x^2-y^2}$ -wave Zeeman field.

1. The case of strongly coupled superconductivity

We make a short notice on the GL coefficient κ in a d -wave Zeeman field. Equation (45c) explicitly contains the Fermi energy E_{F} , which arises from the derivative of the momentum-dependent field [the first term in Eq. (C11)]. In the main text, we neglected this term since weakly coupled superconductors satisfy $T_{\text{c0}} \ll E_{\text{F}}$.

Here, we consider strongly coupled superconductors where the transition temperature T_{c0} is comparable to the Fermi energy T_{c0} . Figure 8 show a phase diagram for $E_{\text{F}}/T_{\text{c0}} = 1$.

In this case, the zeros of κ (green dash-dotted line) become a convex curve upward, while those are a straight line in the weak-coupling limit [Fig. 5(b)]. Therefore, the FF state would be stabilized in the intermediate field regime between the blue and green lines. In a higher Zeeman field, however, the coefficient β also flips to negative; then the amplitude-modulated superconductivity becomes more stable. Although this behavior does not describe our results in Fig. 4, this may correspond to a previous theoretical analysis reporting the transition from the FF state to the PDW state by changing the chemical potential [30].

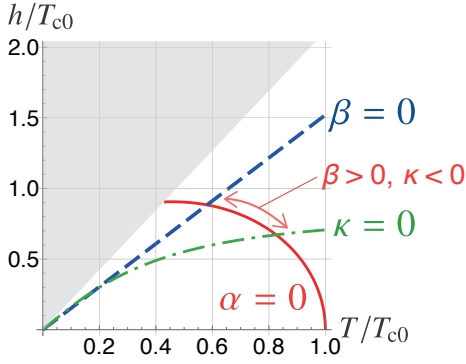


FIG. 8. T - h phase diagram in the continuum model with a d -wave Zeeman field, for strongly coupled superconductivity. As in Fig. 5, the $\alpha = 0$ lines are unreliable when h/T is large (dark shaded areas) since we truncate the infinite series after 100 terms.

2. Integral formulas

We here introduce some integral formulas that are used in the analytical calculations above. First, we show integrals with respect to the energy ξ . Let a and b be arbitrary real numbers. Then the following equations are satisfied:

$$\int_{-\infty}^{\infty} d\xi \frac{1}{[\xi - (i\omega_n + a)][\xi - (-i\omega_n + b)]} = \frac{\pi}{|\omega_n| + i\frac{b-a}{2} \text{sgn}(\omega_n)}, \quad (\text{C13})$$

$$\int_{-\infty}^{\infty} d\xi \frac{1}{[\xi - (i\omega_n + a)]^2 [\xi - (-i\omega_n + b)]^2} = \frac{\pi/2}{[|\omega_n| + i\frac{b-a}{2} \text{sgn}(\omega_n)]^3}, \quad (\text{C14})$$

which are easily proved by using the residue theorem.

Next, we introduce integrals with respect to the angle θ_k . Let l be an integer greater than or equal to 1. Then

$$\int_0^{2\pi} \frac{d\theta_k}{2\pi} \cos^{2l}(2\theta_k) = \frac{(2l)!}{2^{2l}(l!)^2}, \quad (\text{C15})$$

$$\int_0^{2\pi} \frac{d\theta_k}{2\pi} \cos^{2l}(2\theta_k) \cos^2 \theta_k = \int_0^{2\pi} \frac{d\theta_k}{2\pi} \cos^{2l}(2\theta_k) \sin^2 \theta_k = \frac{(2l)!}{2^{2l+1}(l!)^2}, \quad (\text{C16})$$

$$\begin{aligned} & \int_0^{2\pi} \frac{d\theta_k}{2\pi} \cos^{2l-1}(2\theta_k) \sin^2 \theta_k (\sin^2 \theta_k - 3 \cos^2 \theta_k) \\ &= \int_0^{2\pi} \frac{d\theta_k}{2\pi} \cos^{2l-1}(2\theta_k) \cos^2 \theta_k (3 \sin^2 \theta_k - \cos^2 \theta_k) \\ &= -\frac{(2l)!}{2^{2l+1}(l!)^2}, \end{aligned} \quad (\text{C17})$$

are satisfied.

-
- [1] Y. Noda, K. Ohno, and S. Nakamura, Momentum-dependent band spin splitting in semiconducting MnO_2 : a density functional calculation, *Phys. Chem. Chem. Phys.* **18**, 13294 (2016).
- [2] T. Okugawa, K. Ohno, Y. Noda, and S. Nakamura, Weakly spin-dependent band structures of antiferromagnetic perovskite LaMO_3 ($M = \text{Cr, Mn, Fe}$), *J. Phys.: Condens. Matter* **30**, 075502 (2018).
- [3] K.-H. Ahn, A. Hariki, K.-W. Lee, and J. Kuneš, Antiferromagnetism in RuO_2 as d -wave Pomeranchuk instability, *Phys. Rev. B* **99**, 184432 (2019).
- [4] M. Naka, S. Hayami, H. Kusunose, Y. Yanagi, Y. Motome, and H. Seo, Spin current generation in organic antiferromagnets, *Nat. Commun.* **10**, 4305 (2019).
- [5] S. Hayami, Y. Yanagi, and H. Kusunose, Momentum-Dependent Spin Splitting by Collinear Antiferromagnetic Ordering, *J. Phys. Soc. Jpn.* **88**, 123702 (2019).
- [6] I. V. Solovyev, Magneto-optical effect in the weak ferromagnets LaMO_3 ($M = \text{Cr, Mn, and Fe}$), *Phys. Rev. B* **55**, 8060 (1997).
- [7] L. Šmejkal, R. González-Hernández, T. Jungwirth, and J. Sinova, Crystal time-reversal symmetry breaking and spontaneous Hall effect in collinear antiferromagnets, *Sci. Adv.* **6**, eaaz8809 (2020).
- [8] M. Naka, S. Hayami, H. Kusunose, Y. Yanagi, Y. Motome, and H. Seo, Anomalous Hall effect in κ -type organic antiferromagnets, *Phys. Rev. B* **102**, 075112 (2020).
- [9] L. Šmejkal, J. Sinova, and T. Jungwirth, Beyond Conventional Ferromagnetism and Antiferromagnetism: A Phase with Non-relativistic Spin and Crystal Rotation Symmetry, *Phys. Rev. X* **12**, 031042 (2022).
- [10] L. Šmejkal, J. Sinova, and T. Jungwirth, Emerging Research Landscape of Altermagnetism, *Phys. Rev. X* **12**, 040501 (2022).
- [11] H. Seo and M. Naka, Antiferromagnetic State in κ -type Molecular Conductors: Spin Splitting and Mott Gap, *J. Phys. Soc. Jpn.* **90**, 064713 (2021).
- [12] M. Naka, Y. Motome, and H. Seo, Perovskite as a spin current generator, *Phys. Rev. B* **103**, 125114 (2021).
- [13] M. Naka, Y. Motome, and H. Seo, Altermagnetic perovskites, *npj Spintronics* **3**, 1 (2025).
- [14] A. Hariki, A. Dal Din, O. J. Amin, T. Yamaguchi, A. Badura, D. Krieger, K. W. Edmonds, R. P. Campion, P. Wadley, D. Backes, L. S. I. Veiga, S. S. Dhesi, G. Springholz, L. Šmejkal, K. Výborný, T. Jungwirth, and J. Kuneš, X-Ray Magnetic Cir-

- cular Dichroism in Altermagnetic α -MnTe, *Phys. Rev. Lett.* **132**, 176701 (2024).
- [15] R. D. Gonzalez Betancourt, J. Zubáč, R. Gonzalez-Hernandez, K. Geishendorf, Z. Šobáň, G. Springholz, K. Olejník, L. Šmejkal, J. Sinova, T. Jungwirth, S. T. B. Goennenwein, A. Thomas, H. Reichlová, J. Železný, and D. Kriegner, Spontaneous Anomalous Hall Effect Arising from an Unconventional Compensated Magnetic Phase in a Semiconductor, *Phys. Rev. Lett.* **130**, 036702 (2023).
- [16] J. Krempaský, L. Šmejkal, S. W. D'Souza, M. Hajlaoui, G. Springholz, K. Uhlířová, F. Alarab, P. C. Constantinou, V. Strocov, D. Usanov, W. R. Pudelko, R. González-Hernández, A. Birk Hellenes, Z. Jansa, H. Reichlová, Z. Šobáň, R. D. Gonzalez Betancourt, P. Wadley, J. Sinova, D. Kriegner, J. Minár, J. H. Dil, and T. Jungwirth, Altermagnetic lifting of Kramers spin degeneracy, *Nature* **626**, 517–522 (2024).
- [17] T. Osumi, S. Souma, T. Aoyama, K. Yamauchi, A. Honma, K. Nakayama, T. Takahashi, K. Ohgushi, and T. Sato, Observation of a giant band splitting in altermagnetic MnTe, *Phys. Rev. B* **109**, 115102 (2024).
- [18] Z. Liu, M. Ozeki, S. Asai, S. Itoh, and T. Masuda, Chiral Split Magnon in Altermagnetic MnTe, *Phys. Rev. Lett.* **133**, 156702 (2024).
- [19] M.-T. Suzuki, T. Koretsune, M. Ochi, and R. Arita, Cluster multipole theory for anomalous Hall effect in antiferromagnets, *Phys. Rev. B* **95**, 094406 (2017).
- [20] M.-T. Suzuki, T. Nomoto, R. Arita, Y. Yanagi, S. Hayami, and H. Kusunose, Multipole expansion for magnetic structures: A generation scheme for a symmetry-adapted orthonormal basis set in the crystallographic point group, *Phys. Rev. B* **99**, 174407 (2019).
- [21] S. Hayami, M. Yatsushiro, Y. Yanagi, and H. Kusunose, Classification of atomic-scale multipoles under crystallographic point groups and application to linear response tensors, *Phys. Rev. B* **98**, 165110 (2018).
- [22] H. Watanabe and Y. Yanase, Group-theoretical classification of multipole order: Emergent responses and candidate materials, *Phys. Rev. B* **98**, 245129 (2018).
- [23] P. Fulde and R. A. Ferrell, Superconductivity in a Strong Spin-Exchange Field, *Phys. Rev.* **135**, A550 (1964).
- [24] A. I. Larkin and Y. N. Ovchinnikov, Nonuniform state of superconductors, *Zh. Eksp. Teor. Fiz.* **47**, 1136 (1964), [*Sov. Phys. JETP* **20**, 762 (1965)].
- [25] S. Sumita, M. Naka, and H. Seo, Fulde-Ferrell-Larkin-Ovchinnikov state induced by antiferromagnetic order in κ -type organic conductors, *Phys. Rev. Res.* **5**, 043171 (2023).
- [26] S.-B. Zhang, L.-H. Hu, and T. Neupert, Finite-momentum Cooper pairing in proximitized altermagnets, *Nat. Commun.* **15**, 1801 (2024).
- [27] D. Chakraborty and A. M. Black-Schaffer, Zero-field finite-momentum and field-induced superconductivity in altermagnets, *Phys. Rev. B* **110**, L060508 (2024).
- [28] D. Chakraborty and A. M. Black-Schaffer, Constraints on superconducting pairing in altermagnets, [arXiv:2408.03999](https://arxiv.org/abs/2408.03999).
- [29] D. Chakraborty and A. M. Black-Schaffer, Perfect superconducting diode effect in altermagnets, [arXiv:2408.07747](https://arxiv.org/abs/2408.07747).
- [30] G. Sim and J. Knolle, Pair Density Waves and Supercurrent Diode Effect in Altermagnets, [arXiv:2407.01513](https://arxiv.org/abs/2407.01513).
- [31] S. Hong, M. J. Park, and K.-M. Kim, Unconventional p -wave and finite-momentum superconductivity induced by altermagnetism through the formation of Bogoliubov Fermi surface, *Phys. Rev. B* **111**, 054501 (2025).
- [32] K. Mukasa and Y. Masaki, Finite-momentum Superconductivity in Two-dimensional Altermagnets with a Rashba-type Spin–Orbit Coupling, *J. Phys. Soc. Jpn.* **94**, 064705 (2025).
- [33] I. V. Iorsh, Electron pairing by dispersive phonons in altermagnets: Reentrant superconductivity and continuous transition to finite momentum superconducting state, *Phys. Rev. B* **111**, L220503 (2025).
- [34] H. Hu, Z. Liu, and X.-J. Liu, Unconventional superconductivity of an altermagnetic metal: Polarized BCS and inhomogeneous Fulde-Ferrell-Larkin-Ovchinnikov states, [arXiv:2505.10196](https://arxiv.org/abs/2505.10196).
- [35] H. Hu and X.-J. Liu, Quantum Lifshitz points in an altermagnetic metal, [arXiv:2505.10242](https://arxiv.org/abs/2505.10242).
- [36] R. Soto-Garrido and E. Fradkin, Pair-density-wave superconducting states and electronic liquid-crystal phases, *Phys. Rev. B* **89**, 165126 (2014).
- [37] J. Gukelberger, E. Kozik, L. Pollet, N. Prokof'ev, M. Sigrist, B. Svistunov, and M. Troyer, p -Wave Superfluidity by Spin-Nematic Fermi Surface Deformation, *Phys. Rev. Lett.* **113**, 195301 (2014).
- [38] H. Shimahara, Structure of the Fulde-Ferrell-Larkin-Ovchinnikov State in Two-Dimensional Superconductors, *J. Phys. Soc. Jpn.* **67**, 736 (1998).
- [39] Y. Matsuda and H. Shimahara, Fulde–Ferrell–Larkin–Ovchinnikov State in Heavy Fermion Superconductors, *J. Phys. Soc. Jpn.* **76**, 051005 (2007).
- [40] A. I. Buzdin and H. Kachkachi, Generalized Ginzburg-Landau theory for nonuniform FFLO superconductors, *Phys. Lett. A* **225**, 341 (1997).
- [41] D. F. Agterberg and K. Yang, The effect of impurities on Fulde-Ferrell-Larkin-Ovchinnikov superconductors, *J. Phys. Condens. Matter* **13**, 9259 (2001).
- [42] T. A. Maier and S. Okamoto, Weak-coupling theory of neutron scattering as a probe of altermagnetism, *Phys. Rev. B* **108**, L100402 (2023).
- [43] M. Roig, A. Kreisel, Y. Yu, B. M. Andersen, and D. F. Agterberg, Minimal models for altermagnetism, *Phys. Rev. B* **110**, 144412 (2024).
- [44] We here do not take into account symmetry operators that acts only on SOC-free systems. In other words, we do not consider a spin point group.
- [45] S. Sumita, https://github.com/shuntarosumita/altermagnet_SC (2025).
- [46] L. P. Gor'kov, Microscopic derivation of the Ginzburg-Landau equations in the theory of superconductivity, *Zh. Eksp. Teor. Fiz.* **36**, 1918 (1959), [*Sov. Phys. JETP* **36**, 1364 (1959)].
- [47] Y. Ren, J.-H. Xu, and C. S. Ting, Ginzburg-Landau Equations and Vortex Structure of a $d_{x^2-y^2}$ Superconductor, *Phys. Rev. Lett.* **74**, 3680 (1995).
- [48] D. L. Feder and C. Kallin, Microscopic derivation of the Ginzburg-Landau equations for a d -wave superconductor, *Phys. Rev. B* **55**, 559 (1997).
- [49] E. Wigner, On the Quantum Correction For Thermodynamic Equilibrium, *Phys. Rev.* **40**, 749 (1932).
- [50] M. Houzet and V. P. Mineev, Interplay of paramagnetic, orbital, and impurity effects on the phase transition of a normal metal to the superconducting state, *Phys. Rev. B* **74**, 144522 (2006).
- [51] S. Chourasia, A. Svetogorov, A. Kamra, and W. Belzig, Thermodynamic properties of a superconductor interfaced with an altermagnet, *Phys. Rev. B* **111**, 224503 (2025).
- [52] E. Bauer and M. Sigrist, eds., *Non-Centrosymmetric Superconductors*, Lecture Notes in Physics (Springer Berlin, Heidelberg, 2012).
- [53] R. Wakatsuki, Y. Saito, S. Hoshino, Y. M. Itahashi, T. Ideue, M. Ezawa, Y. Iwasa, and N. Nagaosa, Nonreciprocal charge transport in noncentrosymmetric superconductors, *Sci. Adv.* **3**, e1602390 (2017).

- [54] R. Wakatsuki and N. Nagaosa, Nonreciprocal Current in Noncentrosymmetric Rashba Superconductors, *Phys. Rev. Lett.* **121**, 026601 (2018).
- [55] D. Saint-James, G. Sarma, and E. J. Thomas, *Type II Superconductivity* (Oxford, 1969).
- [56] H. Shimahara, Fulde-Ferrell state in quasi-two-dimensional superconductors, *Phys. Rev. B* **50**, 12760 (1994).
- [57] K. Yang and S. L. Sondhi, Response of a $d_{x^2-y^2}$ superconductor to a Zeeman magnetic field, *Phys. Rev. B* **57**, 8566 (1998).
- [58] V. M. Edelstein, Characteristics of the Cooper pairing in two-dimensional noncentrosymmetric electron systems, *Zh. Eksp. Teor. Fiz.* **95**, 2151 (1989), [*Sov. Phys. JETP* **68**, 1244 (1989)].
- [59] V. P. Mineev and K. V. Samokhin, Helical phases in superconductors, *Zh. Eksp. Teor. Fiz.* **105**, 747 (1994), [*JETP* **78**, 401 (1994)].
- [60] D. Agterberg, Novel magnetic field effects in unconventional superconductors, *Physica C* **387**, 13 (2003).
- [61] O. V. Dimitrova and M. V. Feigel'man, Phase diagram of a surface superconductor in parallel magnetic field, *JETP Lett.* **78**, 637 (2003).
- [62] K. V. Samokhin, Magnetic properties of superconductors with strong spin-orbit coupling, *Phys. Rev. B* **70**, 104521 (2004).
- [63] R. P. Kaur, D. F. Agterberg, and M. Sigrist, Helical Vortex Phase in the Noncentrosymmetric CePt₃Si, *Phys. Rev. Lett.* **94**, 137002 (2005).
- [64] D. F. Agterberg and R. P. Kaur, Magnetic-field-induced helical and stripe phases in Rashba superconductors, *Phys. Rev. B* **75**, 064511 (2007).
- [65] O. Dimitrova and M. V. Feigel'man, Theory of a two-dimensional superconductor with broken inversion symmetry, *Phys. Rev. B* **76**, 014522 (2007).
- [66] V. P. Mineev and K. V. Samokhin, Nonuniform states in noncentrosymmetric superconductors: Derivation of Lifshitz invariants from microscopic theory, *Phys. Rev. B* **78**, 144503 (2008).
- [67] M. Smidman, M. B. Salamon, H. Q. Yuan, and D. F. Agterberg, Superconductivity and spin-orbit coupling in noncentrosymmetric materials: a review, *Rep. Prog. Phys.* **80**, 036501 (2017).
- [68] S. Sumita and Y. Yanase, Superconductivity in magnetic multipole states, *Phys. Rev. B* **93**, 224507 (2016).
- [69] S. Sumita, T. Nomoto, and Y. Yanase, Multipole Superconductivity in Nonsymmorphic Sr₂IrO₄, *Phys. Rev. Lett.* **119**, 027001 (2017).
- [70] A. Amin, H. Wu, T. Shishidou, and D. F. Agterberg, Kramers' degenerate magnetism and superconductivity, *Phys. Rev. B* **109**, 024502 (2024).
- [71] S. Kanasugi and Y. Yanase, Anapole superconductivity from \mathcal{PT} -symmetric mixed-parity interband pairing, *Communications Physics* **5**, 39 (2022).
- [72] T. Kitamura, S. Kanasugi, M. Chazono, and Y. Yanase, Quantum geometry induced anapole superconductivity, *Phys. Rev. B* **107**, 214513 (2023).
- [73] A. Daido, Y. Yanase, and K. T. Law, Nonreciprocal Current-induced Zero-Resistance State in Valley-Polarized Superconductors, [arXiv:2503.16923](https://arxiv.org/abs/2503.16923).
- [74] In particular, terms with the second order in η and *linear* in spatial gradient are called the Lifshitz invariants.
- [75] K. Yang and D. F. Agterberg, Josephson Effect in Fulde-Ferrell-Larkin-Ovchinnikov Superconductors, *Phys. Rev. Lett.* **84**, 4970 (2000).
- [76] Y. Kim, M. J. Park, and M. J. Gilbert, Probing unconventional superconductivity in inversion-symmetric doped Weyl semimetal, *Phys. Rev. B* **93**, 214511 (2016).
- [77] S. Yoshida, K. Yada, and Y. Tanaka, Theory of a pair density wave on a quasi-one-dimensional lattice in the Hubbard model, *Phys. Rev. B* **104**, 094506 (2021).
- [78] M. Wallerberger, S. Badr, S. Hoshino, S. Huber, F. Kakizawa, T. Koretsune, Y. Nagai, K. Nogaki, T. Nomoto, H. Mori, J. Otsuki, S. Ozaki, T. Plaikner, R. Sakurai, C. Vogel, N. Witt, K. Yoshimi, and H. Shinaoka, sparse-ir: Optimal compression and sparse sampling of many-body propagators, *SoftwareX* **21**, 101266 (2023).
- [79] T. Wang, T. Nomoto, Y. Nomura, H. Shinaoka, J. Otsuki, T. Koretsune, and R. Arita, Efficient ab initio Migdal-Eliashberg calculation considering the retardation effect in phonon-mediated superconductors, *Phys. Rev. B* **102**, 134503 (2020).
- [80] H. Shinaoka, J. Otsuki, M. Ohzeki, and K. Yoshimi, Compressing Green's function using intermediate representation between imaginary-time and real-frequency domains, *Phys. Rev. B* **96**, 035147 (2017).
- [81] J. Li, M. Wallerberger, N. Chikano, C.-N. Yeh, E. Gull, and H. Shinaoka, Sparse sampling approach to efficient ab initio calculations at finite temperature, *Phys. Rev. B* **101**, 035144 (2020).
- [82] When the vector potential $A(\mathbf{R})$ is taken into account, one should replace the spatial derivative $\nabla_{\mathbf{R}}$ with the covariant derivative $\mathbf{D}_{\mathbf{R}} := \nabla_{\mathbf{R}} - i\frac{2e}{\hbar c}\mathbf{A}(\mathbf{R})$ in the final expression.